Studies of Nonlinear Phenomena in Sensory Systems

A Thesis

submitted to
Indian Institute of Science Education and Research Pune
in partial fulfillment of the requirements for the
BS-MS Dual Degree Programme

by

Ayan Biswas

Indian Institute of Science Education and Research Pune
Dr. Homi Bhabha Road,
Pashan, Pune 411008, INDIA.

December, 2022

Supervisor: Prof Janaki Balakrishnan

Certificate

This is to certify that this dissertation entitled Studies of Nonlinear Phenomena in Sensory Systems, towards the partial fulfilment of the BS-MS dual degree programme at the Indian Institute of Science Education and Research, Pune represents study/work carried out by Ayan Biswas, for Indian Institute of Science Education and Research under the supervision of Prof Janaki Balakrishnan, Professor and Head, Complex Systems Programme at National Institute of Advanced Studies, Bangalore, during the academic year 2021-2022.

B. Janaki

Prof Janaki Balakrishnan

Committee:

Prof Janaki Balakrishnan

Prof M S Santhanam

This thesis is dedicated to:
My family, friends, teachers and mentors

Declaration

I hereby declare that the matter embodied in the report entitled Studies of Nonlinear Phenomena in Sensory Systems are the results of the work carried out by me at the Complex Systems Programme, National Institute of Advanced Studies, Bangalore, under the supervision of Prof Janaki Balakrishnan and the same has not been submitted elsewhere for any other degree.

Ayan Biswas

Acknowledgments

I would like to extend my heartfelt gratitude to my supervisor, Prof Janaki Balakrishnan, for introducing me to an original and interesting research problem through this MS project, and for guiding me through this journey. I would also like to thank Prof M S Santhanam, who kindly agreed to be the expert member in my TAC, for providing me with valuable inputs. I thank the Physics Project Committee: Dr Ashna Bajpai, Dr Sachin Jain and Dr Diptimoy Ghosh for the guidance they offered. I acknowledge DST, government of India for offering me the prestigious INSPIRE SHE scholarship, which supported me through my undergraduate studies. Last but not the least, I would like to thank my parents for allowing me to take this unconventional career path.

Abstract

Neurons being modeled into conductance-based models is extant in the literature since Hodgkin and Huxley. These models often show a rich variety of behaviors as nonlinear dynamical systems. The Hodgkin-Huxley model, being four-dimensional, is difficult to study. Hence several subsequent lower-dimensional models have been suggested. Our aim in this project is to study the dynamical behaviors in a system of two non-identical neurons coupled together. In this venture, we use two such lower-dimensional models called the Hindmarsh-Rose model and the Morris-Lecar model. These two kinds of neurons were coupled unidirectionally and bidirectionally, and the resulting dynamics were studied. Resulting time series of the action potentials in the coupled systems for various sets of parameters and various strengths of coupling have been reported in this study. In some of the cases, the responsible bursting mechanisms have also been reported. We have also briefly covered the relevant concepts, such as the conductance models that have been used, classification of neurons according to their neurocomputational properties, classification of burst mechanisms according to the bifurcations responsible for them etc.

Contents

List of Figures

List of Tables

Chapter 1

Introduction

A biological neuron functions via exchange of ions (like K^+, Ca^{2+} etc.) between its cell body and the surrounding fluid. The fundamental computational unit of a neuron is a 'spike': a sharp, sudden and temporary rise in the membrane voltage (the potential drop across the cell membrane of the neuron is called membrane voltage).

A common question in neuroscience is "What causes a neuron to fire spikes?". Depending on various factors, two neurons can produce same response (in terms of changes in the membrane voltage/spikes) to the same external influence (such as input current fed to the neuron) or different responses to the same external influence. In some cases there might be a threshold input below which the neuron does not fire, or there may be no threshold at all, and what we call 'sub-threshold' oscillations instead. These factors influence the neurocomputational implications of the neuron. [1] [2] A neuron may also exhibit 'bursts' where it fires spikes in groups separated by quiescent periods. Bursts have their significance in high signal-to-noise ratio of information transfer they offer[1], and in facilitating selective communication between neurons [16].

It is very convenient for our understanding to model neurons mathematically: Where we think of neurons as electrical circuits. The ion channels have some conductances and there is some capacitance that the cell membrane offers. Now for any electrical circuit, we may write coupled differential equations that govern it. In case of neurons, the variable in these equations is obviously the membrane potential, along with some other accessory variables like excitation variables, recovery variables, adaptation variables etc. These additional variables

typically take into account things like activation of channels, re-polarization etc. [1]

Thus, once mathematically modelled, we may discuss the neurons in terms of dynamical systems. If we look at a phase portrait of such a neuron, there may be various kinds of fixed points and attractors, and these help us explain neurocomputational behaviors of the neurons. E.g. a stable node will attract nearby trajectories and render the neuron in a quiescent state, whereas a limit cycle attractor will attract nearby trajectories to render the neuron in such a state that its membrane potential varies in a periodic manner, something we refer to as 'tonic spiking'. In this picture, a burst may be attributed to a complicated kind of limit cycle attractor, or spiking modulated by a slow current. Burst is usually observed in models with dimension above 2. In a burst, the start and ending of a spike may be attributed to the neuron being thrown into or out of a spiking regime via bifurcations in the phase portrait. These leads to the discussion on classification of bursts according to bifurcation mechanisms responsible for it [2].

The first mathematical model of neurons was proposed by Hodgkin and Huxley [13] [14]. Their model was a 4-dimensional one, and hence is very complicated to analyse. Later on, several reduced models with 2 or 3 dimensions have been invented to simplify the dynamical systems approach of studying neurons. In this study, we use two such reduced models, namely the Morris-Lecar neuron [3] and the Hindmarsh-Rose neuron [4]. We couple these two unidirectionally and bidirectionally and observe the resulting dynamics. The importance of studying the unidirectional case lies in the fact that here, a neuron capable of bursting (the Morris-Lecar neuron) is being driven by another neuron also capable of showing bursting behaviour. The driver HR neuron not only shows bursting, but it shows a variety of interesting bursts depending on the parameters set in its equations ([8]-[12]). The bidirectional case is important because it captures the scenario where different kinds of neurons reside in the same region and hence are bound to receive the same external stimulation. Bidirectional coupling is also called 'diffusive' coupling. It also must be mentioned that the Morris-Lecar neuron exhibits both type-I and type-II behaviours. Type-I neurons play an important role in low-frequency spikes. On the other hand type-II neurons are responsible for phenomena like cortical gamma oscillations, which plays a key role in focus and memory in the brain [17] [18]. In this study. we have explored both types of ML neurons.

In this thesis, we briefly explain the relevant preliminary concepts in Chapter 1. Then, in Chapter 2, we move to elaborate on the methods we have used to mathematically implement

unidirectional and bidirectional coupling and to detect the bursting mechanisms by observing corresponding phase portraits. In Chapter 4, we report the time series obtained by simulating the coupled systems computationally in various cases, and report the bifurcation mechanisms. In the concluding chapter we lay out the conclusions obtained from the study.

Chapter 2

Preliminaries

2.1 Neurons as dynamical systems

Neurons can be modeled by differential equations on the action potential and some other variables such as recovery variable etc. These equations are often nonlinear. Much insight can be obtained if a dynamical systems approach is taken to study neurons, as they show properties like excitability or bursting which require different bifurcation mechanisms in order to be analysed.

2.1.1 Conductance based models:

In general, a dynamical system is given by a set of differential equations described as

$$\dot{\mathbf{x}} = f(\mathbf{x}) \tag{2.1}$$

Where $\mathbf{x}$ is a vector whose components are the variables of the dynamical system and $f : \mathbb{R}^n \to \mathbb{R}^n$ is a vector-valued function. It's possible to describe a lot of features and phenomena of neurons without imposing any restrictions on f as done by Izhikevich [2].

However, a rather realistic way of modelling neurons is by conductance-based models. The general form of such models is

$$\begin{aligned} \dot{v} &= I - \sum_{i=1}^{n} g_i(\mathbf{x})(v - \mathcal{E}_i) \\ \dot{\mathbf{x}} &= f(v, \mathbf{x}) \end{aligned} \tag{2.2}$$

Where v is the membrane voltage and $x \in \mathbb{R}^k$ is a vector whose k components are recovery variables, gating variables etc. We shall, in brief, try to understand how this form arises.

Action potential is a sudden rise and fall in the membrane voltage across a small patch on the cell membrane of the neuron. Influx and efflux of ions through ion channels on the cell membrane are responsible for this to happen. This action potential travels through ion cascades along the length of the neuron. Trains of such travelling action potentials and the temporal patterns thereof render the neurocomputational properties of the neuron. Activities across a small patch on the neuron cell membrane may be described by an electrical circuit whose two ends are the two sides of the cell membrane (Fig 2.1). The cell membrane is assumed to act like a capacitor C, and the ion channels as conductances g_i. $\mathcal{E}_i$ are equilibrium potentials of the channels, i.e. at that potential the net current across the channel will be zero. It must be noted that the conductances g_i may not follow ohm's law. The conductances may be dependent on the membrane voltage and other factors which influence the flow of ions through the ion channels. Also, since we are looking at a small patch on the membrane, we actually mean current per unit area, capacitance per unit area and conductance per unit area when we say current, capacitance and conductance respectively.

From Fig 2.1, we write the equation for total current across the membrane:

$$\begin{aligned} I &= C\dot{v} + \sum_{i=1}^{n} g_i(v - \mathcal{E}_i) \\ \implies C\dot{v} &= I - \sum_{i=1}^{n} g_i(v - \mathcal{E}_i) \end{aligned} \tag{2.3}$$

And these conductances g_i are dependent on a set other variables given by a vector $\mathbf{x}$ that can, in general vary as in (2.2). An example of how this comes up can be the first-ever model of neuron, namely the Hodgkin-Huxley model. It was formulated by Hodgkin and Huxley in 1952, to describe the squid giant axon:

$$\begin{aligned} C\dot{v} = I - \bar{g}_K n^4 (v - \mathcal{E}_K) - \bar{g}_{Na} m^3 h (v - \mathcal{E}_{Na}) - g_L (v - \mathcal{E}_L) \\ \dot{n} = \alpha_n(V)(1-n) - \beta(v)n \\ \dot{m} = \alpha_n(V)(1-m) - \beta(v)m \\ \dot{h} = \alpha_n(V)(1-h) - \beta(v)h \end{aligned} \tag{2.4}$$

Where

$$\begin{aligned} \alpha_n(v) &= 0.01 \frac{10 - v}{\exp\left(\frac{10-v}{10}\right) - 1} \\ \beta_n(v) &= 0.125 \exp\left(\frac{-v}{80}\right) \\ \alpha_m(v) &= 0.1 \frac{25 - v}{\exp\left(\frac{25-v}{10}\right) - 1} \\ \beta_m(v) &= 4 \exp\left(\frac{-v}{18}\right) \\ \alpha_h(v) &= 0.07 \exp\left(\frac{-v}{20}\right) \\ \beta_h(v) &= \frac{1}{\exp\left(\frac{30-v}{10}\right) + 1} \end{aligned} \tag{2.5}$$

Here n, m, and h are activation variables of K^+ and Na^+ channels and inactivation variable for Na^+ channel respectively. $\bar{g_K}$ and $\bar{g_{Na}}$ are maximal conductances of the populations of K^+ and Na^+ channels respectively. $g_L(v - \mathcal{E}_L)$ is an ohmic leak current, of which the carriers are majorly Cl^- ions.

Maximal Conductance: The maximum conductance that a population of ion channels can have.

Activation and inactivation variables: Voltage-gated ion channels have two kinds of gates sensitive to the membrane voltage: some who activate the gate and some who deactivate the gate. The probability of an activation/inactivation gate being open is called activation/inactivation variable for that gate.

Leak current/conductance: There are some ionn channels which are always open. Their conductance is assumed to be independent of the membrane potential and hence these are ohmic conductances. These are called leak conductances and the current through them is called leak current.

2.1.2 Reduction of neuron models:

The Hodgkin-Huxley equations (2.4) are a set of 4 differential equations, and hence its phase space will be four-dimensional. Four dimensions are very troublesome to deal with. Hence we look for 'minimal' neuron models by attempting to reduce general models.

One such method of reduction is keeping ignoring the contribution of some current or gating variable and checking if the modified system is a valid neuron model. Any valid model of neuron, at the very least, should be capable of showing spiking behaviour, which arises from limit cycles in the phase space. So our minimal model should have at least one limit cycle in some parameter regime. And 'minimal' means that it should not be further reducible. i.e. a model will be minimal only if removing one more current or gating variable renders the system with only equilibrium attractors, thus incapable of spiking.

One such reduced model is the Morris-Lecar model, which we shall be discussing shortly.

2.2 Excitability of neurons

Neurons have two states: quiescence and spiking. Spiking can be transient, repetitive, or there can be periodic transitions between spiking and quiescent states (called bursting). Typically, periodic spikes occur due to presence of a limit cycle attractor in the phase portrait of the dynamical system governing the neuron, while transient spiking corresponds to the system being perturbed from a stable fixed point and jumping to a large trajectory nearby

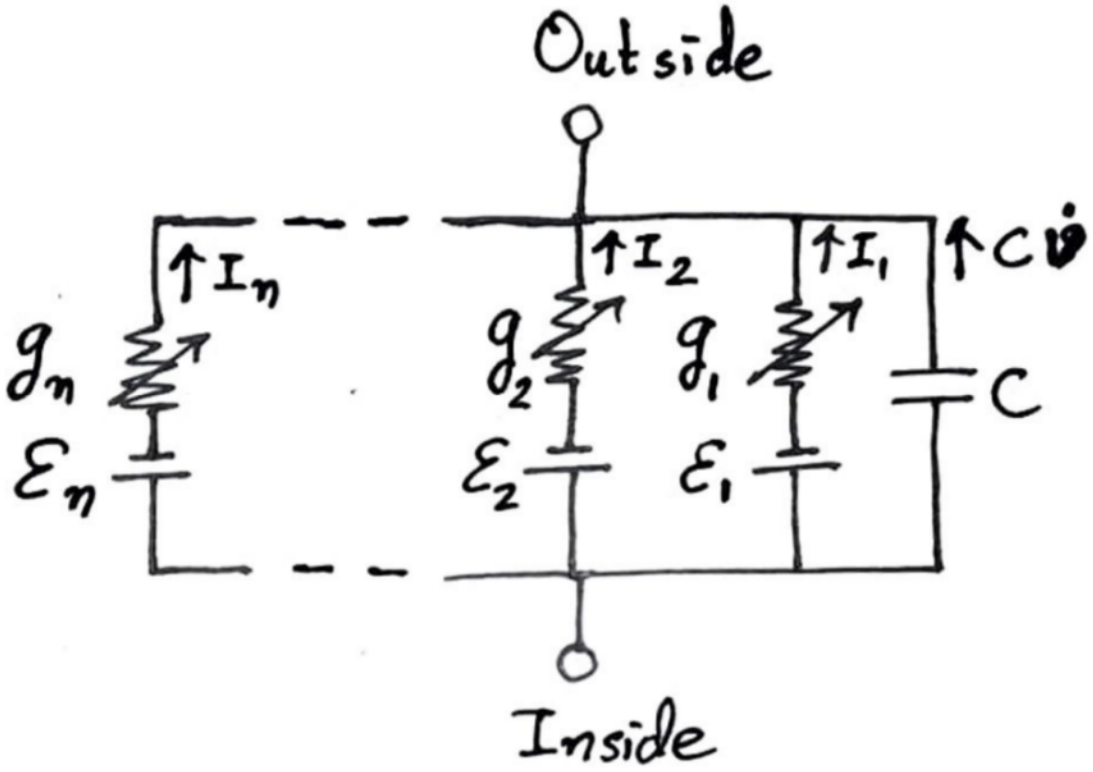

Figure 2.1: The circuit depicting a small patch of the cell membrane

before coming back to the attractor. Some systems have a limit cycle attractor very near to a stable fixed point so that an appropriate perturbation from the stability can make a quiescent neuron to start spiking periodically. This kind of systems are called excitable systems.

2.2.1 Type-I and Type-II Neurons

Excitability may be of three types, according to Hodgkin classification of excitability. The first two classes are nowadays referred to as 'Type-I' and 'Type-II'. From the dynamical systems point of view, this type is determined by the kind of bifurcation the neuron goes through while transitioning between the quiescent state and the spiking state. Typically, the bifurcation responsible for a Type-I excitability is a Saddle-node on invariant circle bifurcation. These neurons are also called 'integrators'. In this case, the neuron is capable of exhibiting arbitrarily small-frequency oscillations. Also, the strength of the input dictates the frequency of spikes.

On the other hand, Andronov-Hopf bifurcations are responsible for Type-II excitability. These neurons, also called 'resonators', produce spikes only in a certain frequency range. These neurons cannot encode input strength into the spiking rate. But these neurons show something called 'subthreshold oscillations'.

To experimentally distinguish between the two, a slowly increasing ramp of current input is applied to the neuron, and the start of the spike is observed.[1] Once the spike appears, the frequency of the spike is also observed with respect to the input current. In case of a type-I neuron, the frequency continuously increases from 0 with increasing current. In a type-II neuron, at a certain value of input current, the neuron starts spiking abruptly with a non-zero frequency. The frequency vs current graphs in both cases are shown in Fig 2.2. Here f is the frequency, I is input current, I_{Th} is the threshold value of input current where the neuron starts spiking.

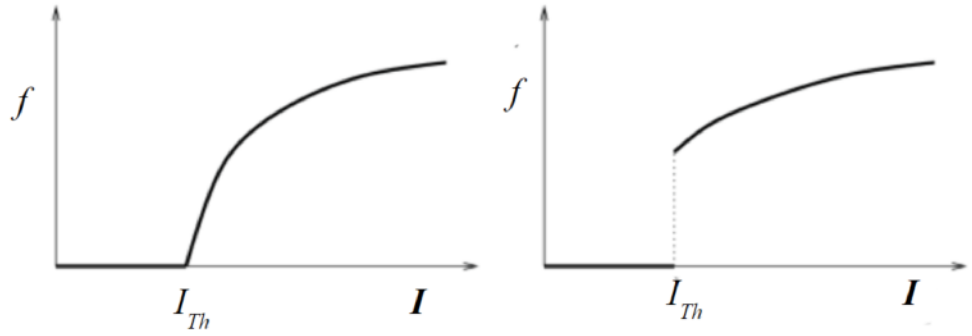

Figure 2.2: frequency vs input current graphs for type-I (left) and type-II (right) neurons

2.2.2 Type-I and type-I neurons from the dynamical systems point of view:

We shall try to understand exactly why type-I and type-II neurons behave the way they do from qualitative study of the phase portraits of their dynamical models. [1]

The Saddle-node-on-invariant-circle (SNIC) bifurcation: Fig 2.3 shows a Saddle-node-on-invariant-circle (SNIC) bifurcation. In this bifurcation, a saddle-node pair appears on a stable limit cycle, and the limit cycle becomes and invariant circle. Spiking trajectories that had been following the stable limit cycle now arrive at the stable node and the neuron becomes quiescent.

Neurons transitioning to spiking state via this bifurcation show arbitrarily low frequency of oscillations, as the frequency of the invariant circle scales as $\sqrt{I - I_b}$ where I is the input current and I_b is the bifurcation value of the input current. This bifurcation is responsible behind type-I neurons.

Andronov-Hopf bifurcation:

Here, a limit cycle combines with a focus. This can be of two types: supercritical and subcritical. In the subcritical case, an unstable limit cycle shrinks and combines with a stable focus, and makes it an unstable focus. In the supercritical case, a stable limit cycle shrinks and combines with an unstable focus, and makes it stable. In any transition from resting to spiking state that occurs through such a bifurcation, the frequency of the spike can start from any arbitrary value, depending on which nearby limit cycle is responsible for

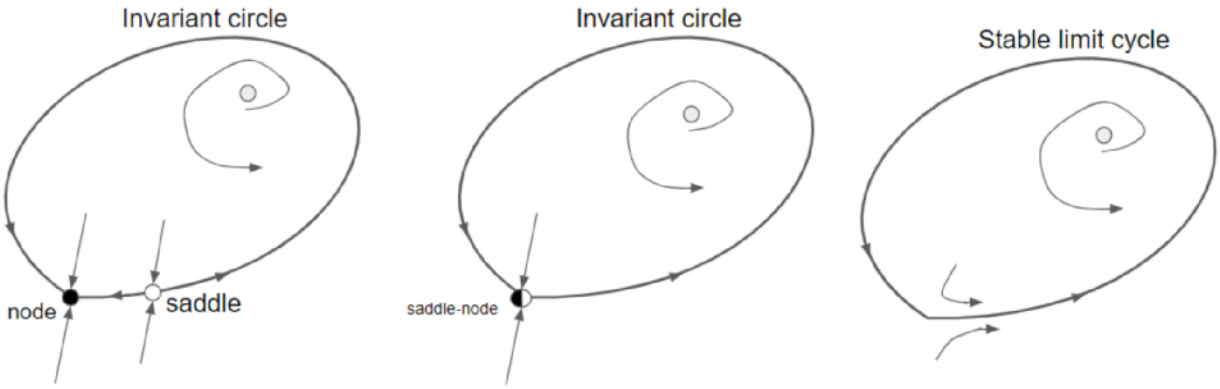

Figure 2.3: SNIC bifurcation

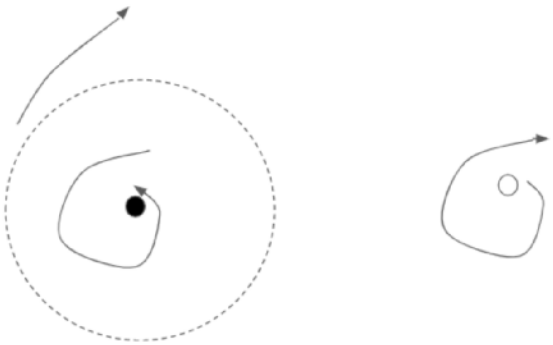

Figure 2.4: Subcritical Hopf bifurcation

the spiking state. This is one of the mechanism behind type-II behavior of neurons.

Saddle-homoclinic orbit bifurcation:

In this context, we should mention another bifurcation that we shall encounter in our discussions: the Saddle-homoclinic orbit bifurcation. Here, a stable limit cycle collides with a saddle and disappears, thus ending a spiking state and making nearby trajectories vulnerable towards ending upon some nearby stable node or focus, thus initiating a resting state.

fold limit cycle bifurcation: In this bifurcation a stable and an unstable limit cycle collide and annihilate each other. At the very point of the bifurcation, there is a special kind of limit cycle called fold limit cycle: trajectories from one side (between inside and outside) are attracted to it and those from the other side are repelled. This is shown in Fig 2.7.

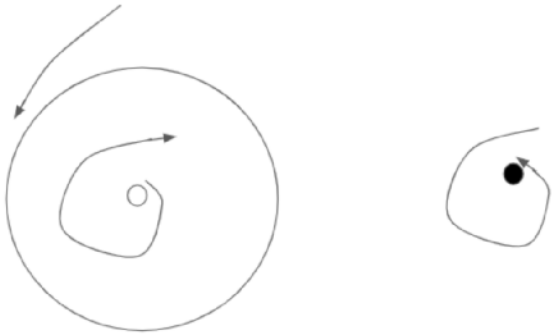

Figure 2.5: Supercritical Hopf bifurcation

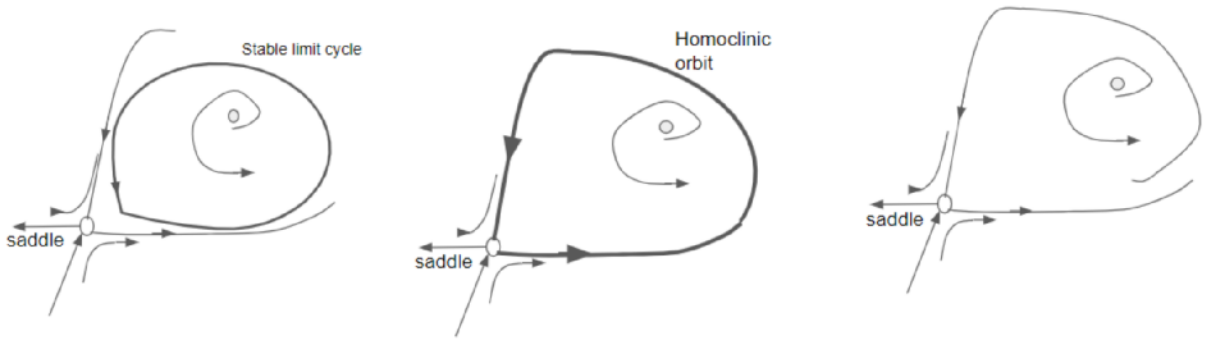

Figure 2.6: Saddle-homoclinic orbit bifurcation

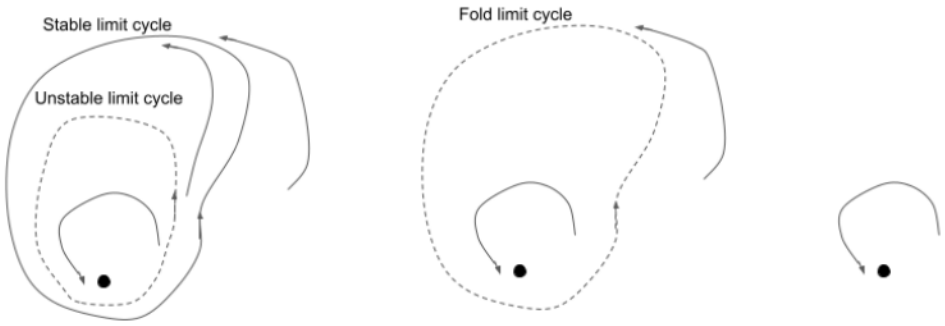

Figure 2.7: Fold limit cycle bifurcation

2.3 The phenomenon of bursting and bifurcation mechanisms governing them

Bursting typically occurs when the system follows a limit cycle attractor which has an oscillatory part as well as a smooth part. These systems can be generically described by a fast spiking subsystem modulated by a slow subsystem. These are called fast-slow bursters:

$$\begin{aligned} \dot{x} &= f(x,u) \\ \dot{u} &= \mu g(x,u) \end{aligned} \tag{2.6}$$

Where the equations respectively describe the fast and slow systems. Now, the onset and disappearance of the spiking in a bursting time series can be attributed to bifurcations in the fast subsystem x with respect to the slow subsystem u, considered as a parameter, and considered in the frozen state (i.e. $\dot{u} = 0$). The parameter μ controls how slow the slow subsystem is, and $0 < \mu << 1$. As u varies slowly with time, it causes the fast subsystem

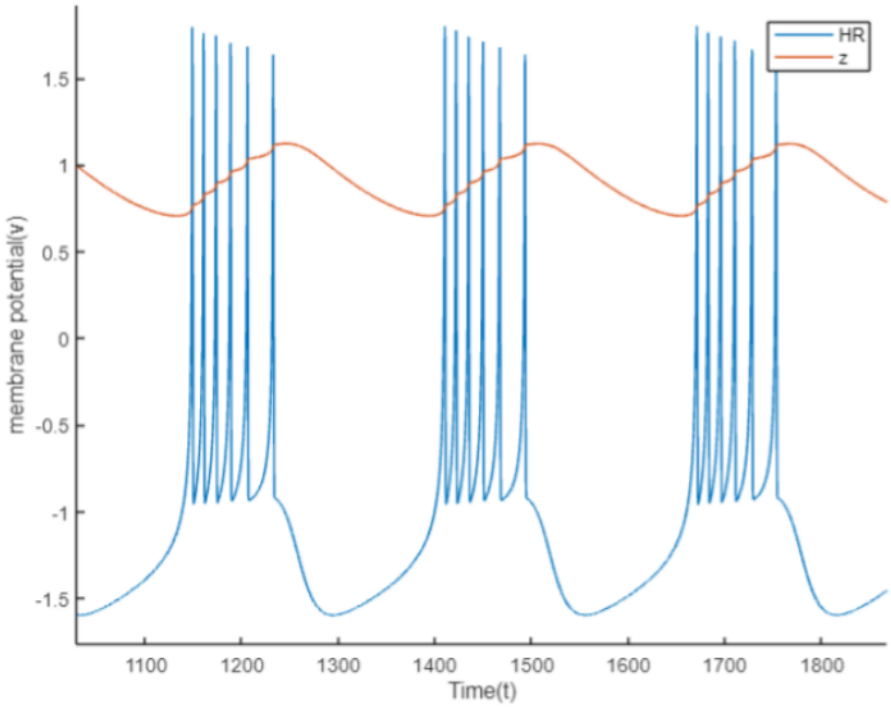

Figure 2.8: Burst in the Hindmarsh-Rose neuron. z is the slow variable here

to move to and fro between spiking and quiescent regimes, and thus we observe groups of spikes punctuated by intermediate quiescent states (Fig 2.8).

2.3.1 Classification of bursters:

Fast-slow burster neurons are named/classified according to the bifurcation mechanisms by which they operate. There are two bifurcations involved in a fast-slow burster: The bifurcation when the fast subsystem moves to the spiking regime from the quiescent region, and the bifurcation when it moves back to the quiescent regime from the spiking regime. A burster is named as follows: e.g. if the bifurcation at the start is fold or saddle-node bifurcation and that at the end is a Hopf bifurcation, then the burster will be named 'fold/Hopf'. Rinzel, Bertram and Izhikevich have exhaustively completed this classification scheme [2].

2.3.2 Significance of bursting:

A single spike may just be noise, but burst indicates that the activity is not just mere noise, since it is a group of repeated spiking. Bursting higher signal-to-noise ratio transmission as compared to spiking. One single spike may fail to induce postsynaptic response, but burst as a bombardment of spikes makes the response more likely, thus serving as a failproof system. Also, burst duration and interburst frequency may carry important information, i.e. bursting can carry more information than spiking.

2.4 Brief review of the Hindmarsh-Rose Model [4]

The Hindmarsh-Rose model of neuron is capable of showing a wide variety of dynamics of the membrane potential. These include interesting cases of bursts as well as some cases of chaotic dynamics ([8]-[12]). The Hindmarsh-Rose Model is governed by the equations

$$\begin{aligned} \dot{v} &= -av^3 + bv^2 + y - z + I \\ \dot{y} &= -dv^2 + c - y \\ \dot{z} &= r[s(v - x_R) - z] \end{aligned} \tag{2.7}$$

Where v is the membrane potential, y and z take into account the transport of ions across the membrane through the ion channels.

2.5 Brief review of the Morris-Lecar Model [3]

Cathy Morris and Harold Lecar devised their eponymous Morris-Lecar model of neuron in 1981. It is a 2-dimensional 'reduced model' and hence is substantially simple to analyse as a dynamical system. This is why, this model is really popular in computational neuroscience. This model is particularly very handy in modelling fast-spiking neurons. A physiological example of such neurons may be the pyramidal neurons in the neocortex. Apart from that,

these neurons can show both type-I and type-II behaviours, depending on the parameters that are set in the equations.[7]

The Morris-Lecar Neuron is governed by the equations

$$\begin{aligned} C\dot{V} &= -g_L(V - V_L) - g_K r(V - V_K) - g_{Ca} m_\infty (V - V_{Ca}) + I \\ \dot{r} &= \lambda(V)(r_\infty - r) \end{aligned} \tag{2.8}$$

Where

$$\begin{aligned} m_\infty(V) &= \frac{1}{2}(1 + tanh(\frac{V - V_1}{V_2})) \\ r_\infty(V) &= \frac{1}{2}(1 + tanh(\frac{V - V_3}{V_4})) \\ \lambda(V) &= \phi cosh(\frac{V - V_3}{2V_4}) \end{aligned} \tag{2.9}$$

The variables and the parameters are as follows: V is the membrane potential, r is the recovery variable, I applied current, C membrane capacitance, the g_L, g_{Ca}, g_K are leak, Ca^{2+} and K^+ conductances through various channels, V_L, V_{Ca}, V_K are equilibrium potential of relevant ion channels; V_1, V_2, V_3, V_4 are tuning parameters for steady state and time constant. ϕ is reference frequency.

Chapter 3

Methods

3.1 Computational Techniques Used:

The differential equations involved were solved in MATLAB using 5th order runge-kutta method. Value of the parameters were borrowed from standard literature[5],[6], as well as tweaked manually to inspect different behavior regimes of the neurons.

3.2 Coupling the neurons

3.2.1 Unidirectionally

In the unidirectional case, a Hindmarsh-Rose neuron drives the Morris-Lecar neuron. Here, the Hindmarsh-Rose neuron is left to follow its usual dynamics independently. A coupling term $\gamma(v_1 - v_2)$ is fed, along with the external current input, to the ML neuron. Here, γ is called the coupling constant, since it controls the strength of the coupling. The overall set

of differential equations depicting this coupled model is given by:

$$\begin{aligned} \dot{v_1} &= -av_1^3 + bv_1^2 + y - z + I \\ \dot{y} &= -dv_1^2 + c - y \\ \dot{z} &= r[s(v_1 - x_R) - z] \\ C\dot{v_2} &= -g_L(v_2 - V_L) - g_K r(v_2 - V_K) - g_{Ca} m_\infty (v_2 - V_{Ca}) + \gamma(v_1 - v_2) \\ \dot{r} &= \lambda(v_2)(r_\infty - r) \end{aligned} \tag{3.1}$$

3.2.2 Bidirectionally

In the bidirectionally coupled case, the action potential of the Hindmarsh-Rose neuron is fed into the Morris-Lecar neuron along with the external stimulus current, and vice versa. So overall, a coupling term $\gamma(v_1 - v_2)$ is fed, along with the external current input I, to both the neurons. Here, γ is the coupling constant. It is worth noting that both the neurons are receiving the same amount of external stimulation, namely I. The overall bidirectionally coupled system is, then, represented by:

$$\begin{aligned} \dot{v_1} &= -av_1^3 + bv_1^2 + y - z + \gamma(v_2 - v_1) + I \\ \dot{y} &= -dv_1^2 + c - y \\ \dot{z} &= r[s(v_1 - x_R) - z] \\ C\dot{v_2} &= -g_L(v_2 - V_L) - g_K r(v_2 - V_K) - g_{Ca} m_\infty (v_2 - V_{Ca}) + \gamma(v_1 - v_2) + I \\ \dot{r} &= \lambda(v_2)(r_\infty - r) \end{aligned} \tag{3.2}$$

3.2.3 Identification of the bifurcation mechanism from phase portraits

Nullclines and phase portraits of the two models: Here we plot the Nullclines of the (Undriven) HIndmarsh-Rose and Morris-Lecar models. These will help us understand the dynamics of the system later when we couple the two neurons.

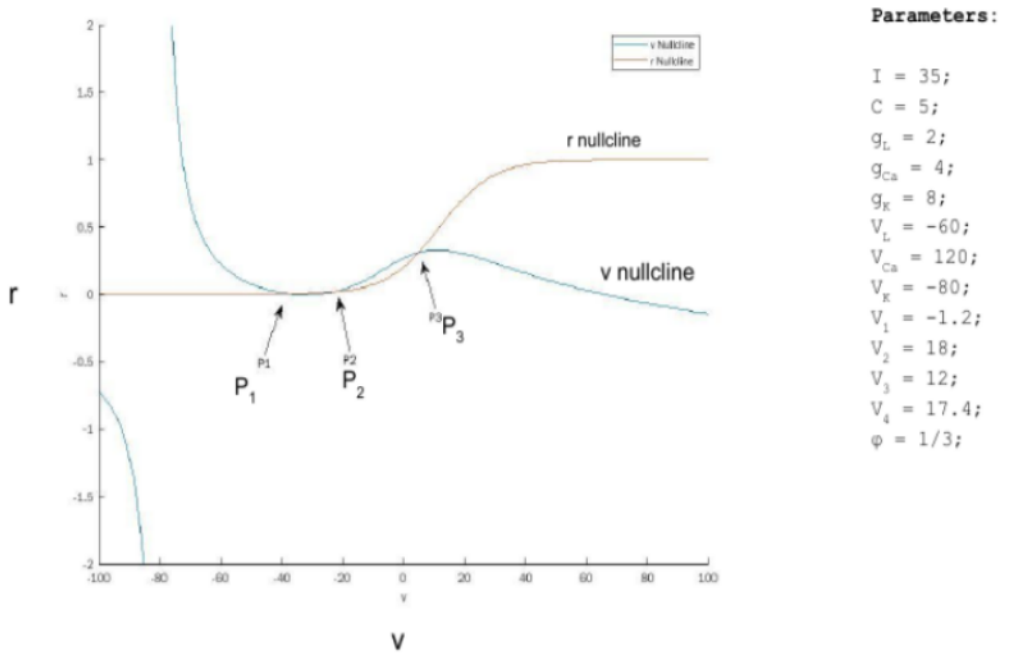

Figure 3.1:
Nullclines of the Morris-Lecar model. In the most general case, there may be 3 fixed points. We mark them by P_1, P_2 and P_3.

Morris-Lecar Model: In the r vs V space, we plot the following equations:

$$\begin{aligned} \dot{V} &= 0 \\ \dot{r} &= 0 \end{aligned} \tag{3.3}$$

Where the variables are as in (2.8)

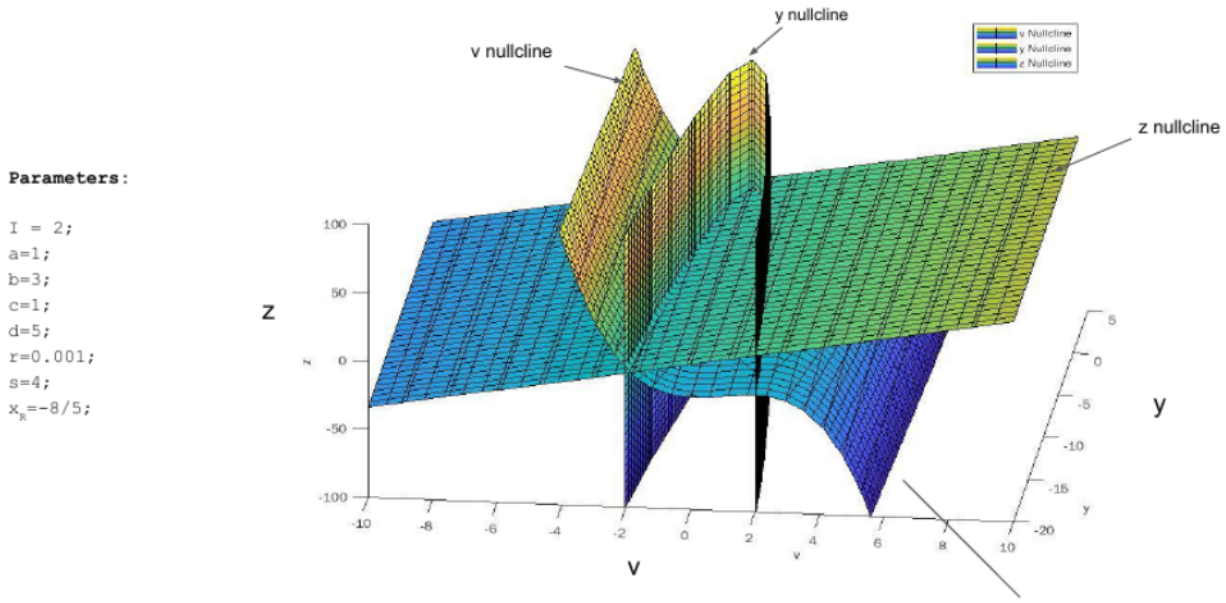

Figure 3.2: Nullclines of the Hindmarsh-Rose model

Hindmarsh-Rose Model: In the $v - z - y$ space, we plot the following equations:

$$\begin{aligned} \dot{v} &= 0 \\ \dot{y} &= 0 \\ \dot{z} &= 0 \end{aligned} \tag{3.4}$$

Where the variables are as in (2.7)

In order to identify the mechanism of bifurcation of any burst that may arise in the driven Morris Lecar neuron in the Unidirectional system, we need to treat the phase portrait and nullclines of the Morris Lecar system as an independent entity and treat the effect of coupling as a variable that causes qualitative changes in the phase portrait/nullclines. To

perform this, we rewrite the last two equations of (3.1) as follows:

$$\begin{aligned} C\dot{v_2} &= -g_L(v_2 - v_L) - g_K r(v_2 - v_K) - g_{Ca} m_\infty (v_2 - v_{Ca}) + F_{coup} \\ \dot{r} &= \lambda(v_2)(r_\infty - r) \end{aligned} \tag{3.5}$$

i.e., we put $F_{coup} = \gamma(v_1 - v_2)$

This method is inspired from a similar method described in a paper by S De and J Balakrishnan [6].

Possible bifurcations in the Unidirectional case for a Type-II Morris-Lecar neuron

Hereafter, we plot the nullclines of the type-II Morris-Lecar system described by (3.5), in the r vs v_2 space, by setting $\dot{v_2} = 0$ and $\dot{r} = 0$

As for the parameters, the parameters used here are borrowed from literature [7]:

$$\begin{aligned} C = 20; g_L = 2; g_{Ca} = 4; g_K = 8; V_L = -60; V_{Ca} = 120; \\ V_K = -84; V_1 = -1.2; V_2 = 18; V_3 = 12; V_4 = 17.4; \phi = 0.23; \end{aligned} \tag{3.6}$$

It can be observed that the phase portrait can be through the following important stages, that dictate the neurocomputational property of the driven ML neuron (Linear stability analyses were done for the fixed points and the eigenvalues have been reported accordingly):

Regime 1: Firstly, there can be a regime where there is only one fixed point P (Fig 3.3), which is a stable focus. And in this regime, all trajectories spiral in towards P.

Regime 2: Then there is this regime where a pair of stable and unstable limit cycles arise out of blue, and now there are two basins separated by the unstable limit cycle (Fig 3.4):

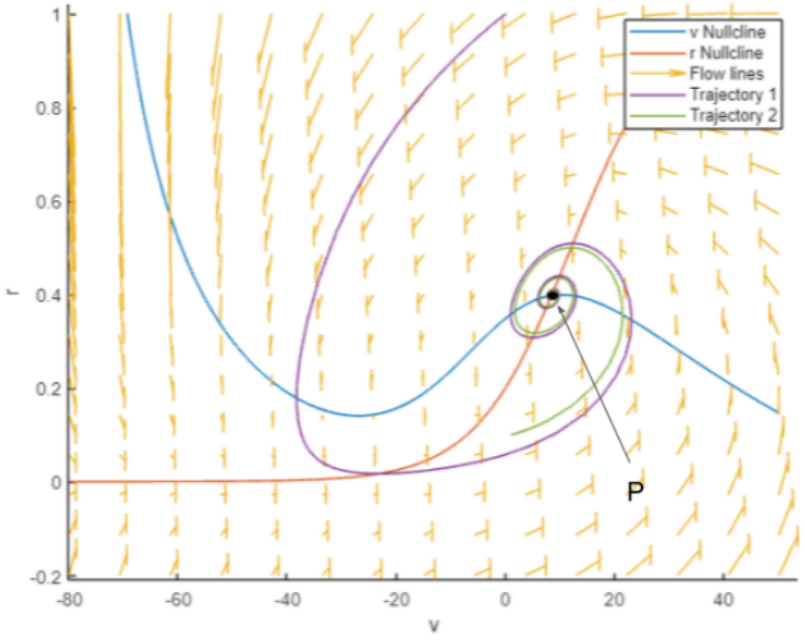

Figure 3.3:
Regime 1: trajectories spiral towards the stable focus (Eigenvalues from Linear Stability Analysis: $-0.0830 + 0.4618i, -0.0830 - 0.4618i$) P. Here, $F_{coup} = 98.56$

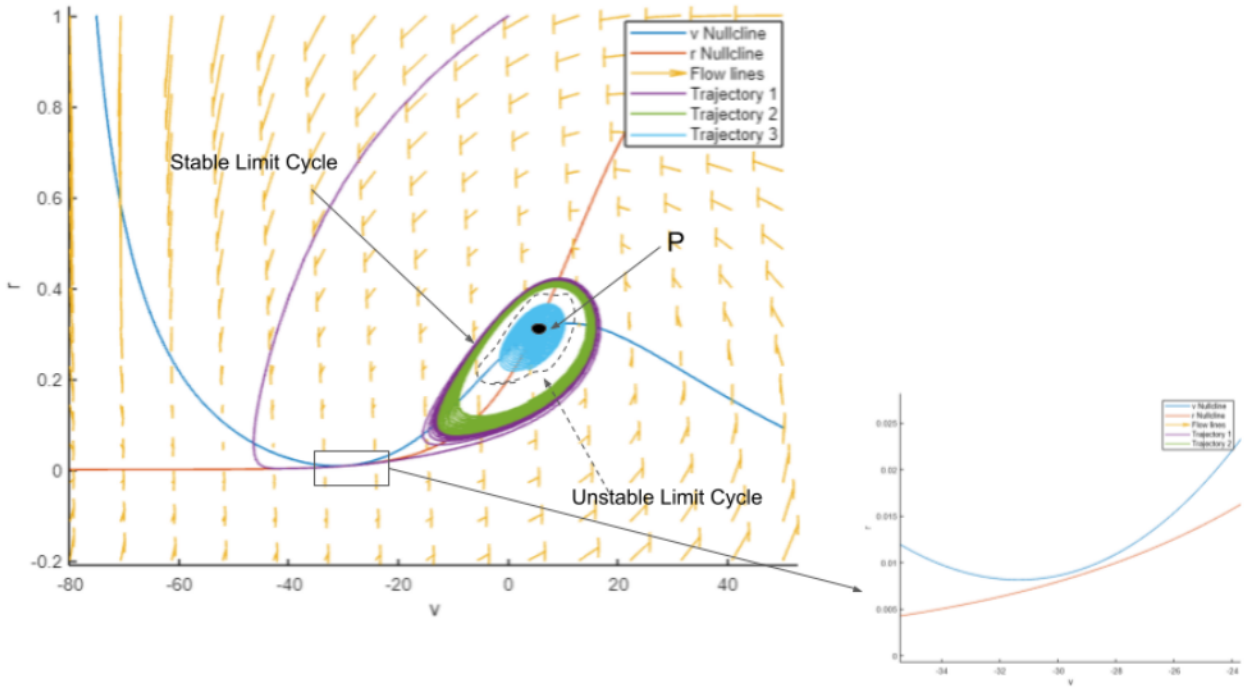

Figure 3.4:
Regime 2: Here $F_{coup} = 40.21$. Eigenvalues from linear stability analysis for P: $-0.0060 + 0.3870i$, $-0.0060 - 0.3870i$

trajectories inside the unstable limit cycle spiral in towards P, which is still a stable node, and trajectories outside the unstable limit cycle are destined to the stable limit cycle. There are no other fixed points than the stable node P, but there is a stable limit cycle now. Thus, in this regime, the neuron is in a bistable state: it may show tonic spiking or quiescence depending on initial conditions. Fig 3.5 and Fig 3.6 show these two cases, illustrating the bistability.

Regime 3: Then comes another regime when the v nullcline intersects the r nullcline at two more points (Fig 3.7), a saddle-node bifurcation occurs, and now there are 3 fixed points: we label them P_1, P_2 and P_3. Out of these, P_1 is a stable node, P_2 is a saddle and P_3 is a stable focus. Depending on initial conditions, some trajectories now may arrive at the stable node P_1 also (here, the purple trajectory). So again, we may observe quiescence or tonic spiking depending on the initial conditions. In terms of neurocomputational implications,

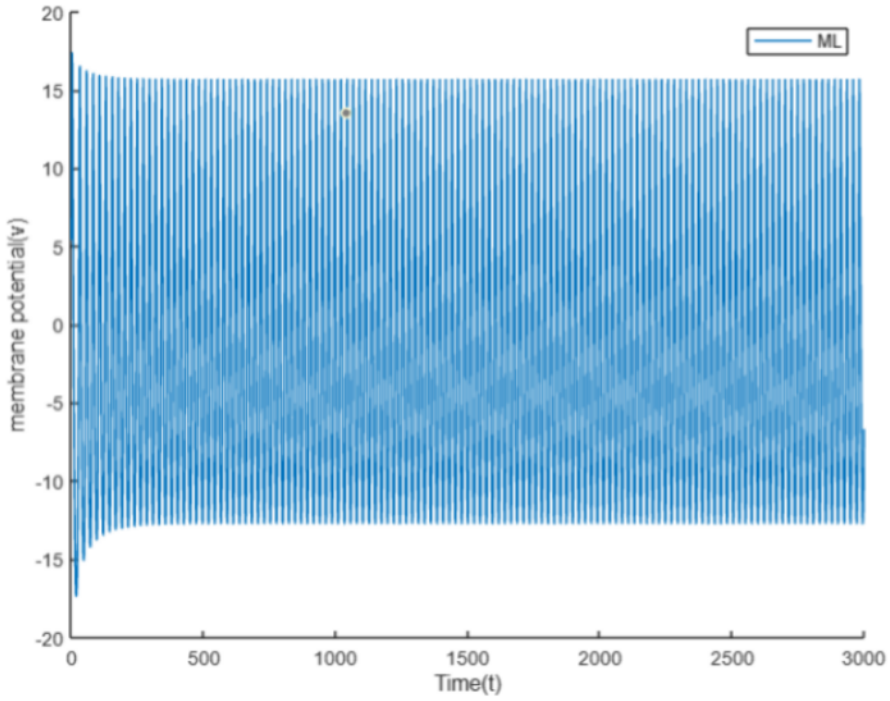

Figure 3.5:
Bistability in regime 2: With $F_{coup} = 40.21$, a trajectory starting from $(v_2, r) = (5.4, 0.1)$ ends up in the stable limit cycle, and hence spiking occurs

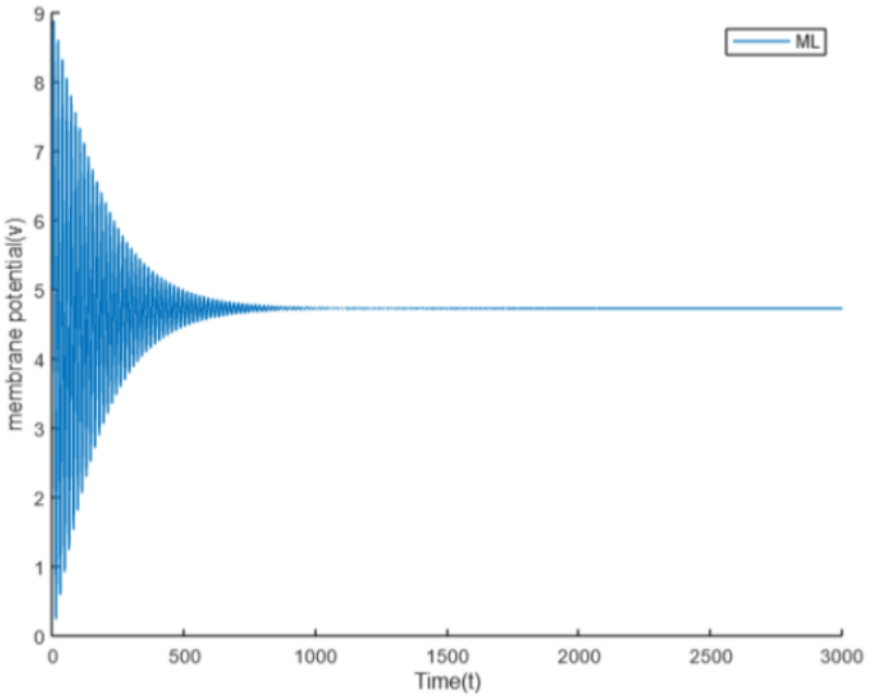

Figure 3.6:
Bistability in regime 2: With $F_{coup} = 40.21$, a trajectory starting from $(v_2, r) = (5, 0.25)$ ends up in the stable focus P, and hence the neuron shows quiescence

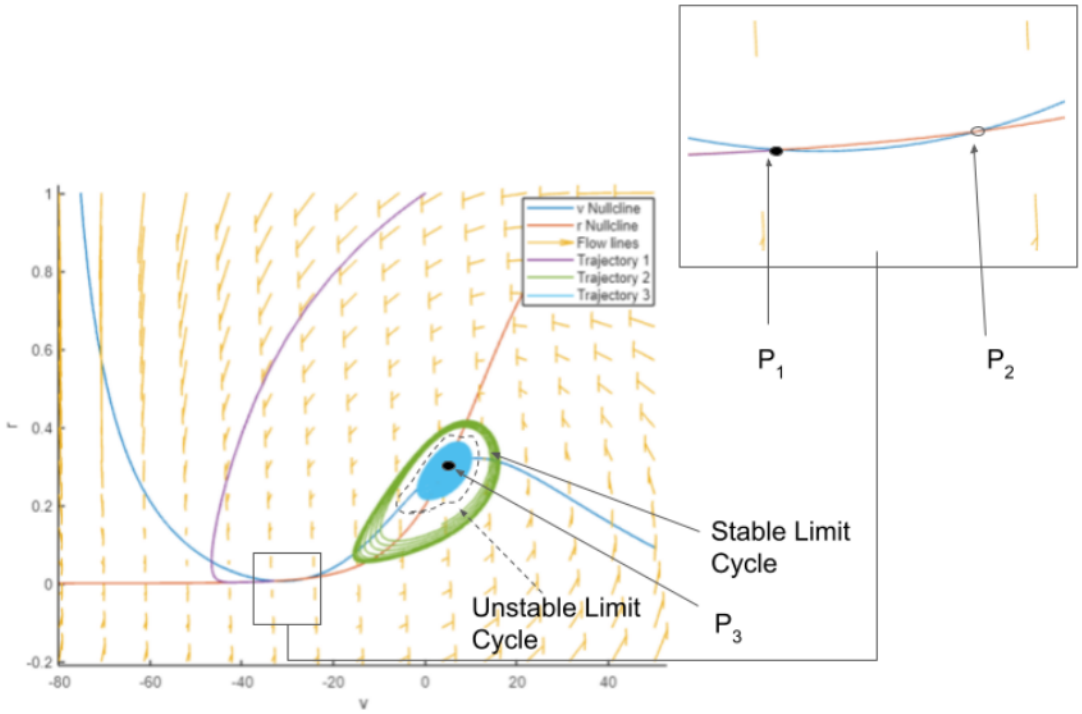

Figure 3.7: Regime 3: A saddle-node bifurcation. Here, $F_{coup} = 39.00$

Table 3.1: Linear stability analysis for Fig 3.7

Point	(v_2^*, r_2^*)	λ_1	λ_2	Type of fixed point
P1	(-32.8756 , 0.0057)	-0.0274	-0.4350	Stable node
P2	(-26.1558 , 0.0123)	0.0334	-0.3529	Saddle
P3	(4.6275 , 0.3000)	-0.0041 + 0.3845i	-0.0041 - 0.3845i	Stable Focus

this regime is essentially the same as Regime 2, but it's just that there are 3 fixed points now, instead of one, and hence there can be two kinds of quiescent states (corresponding to P_1 and P_3 respectively) instead of one, and one tonic spiking state as before, corresponding to the stable limit cycle.

Regime 4: Then, the unstable limit cycle keeps shrinking and dispppears into P_3 by a subcritical Hopf bifurcation (Fig 3.8). Now P_3 becomes an unstable focus. Now there are two options for trajectories to arrive: either the stable limit cycle or the stable node P_1. So again, we may observe quiescence or tonic spiking depending on the initial conditions.

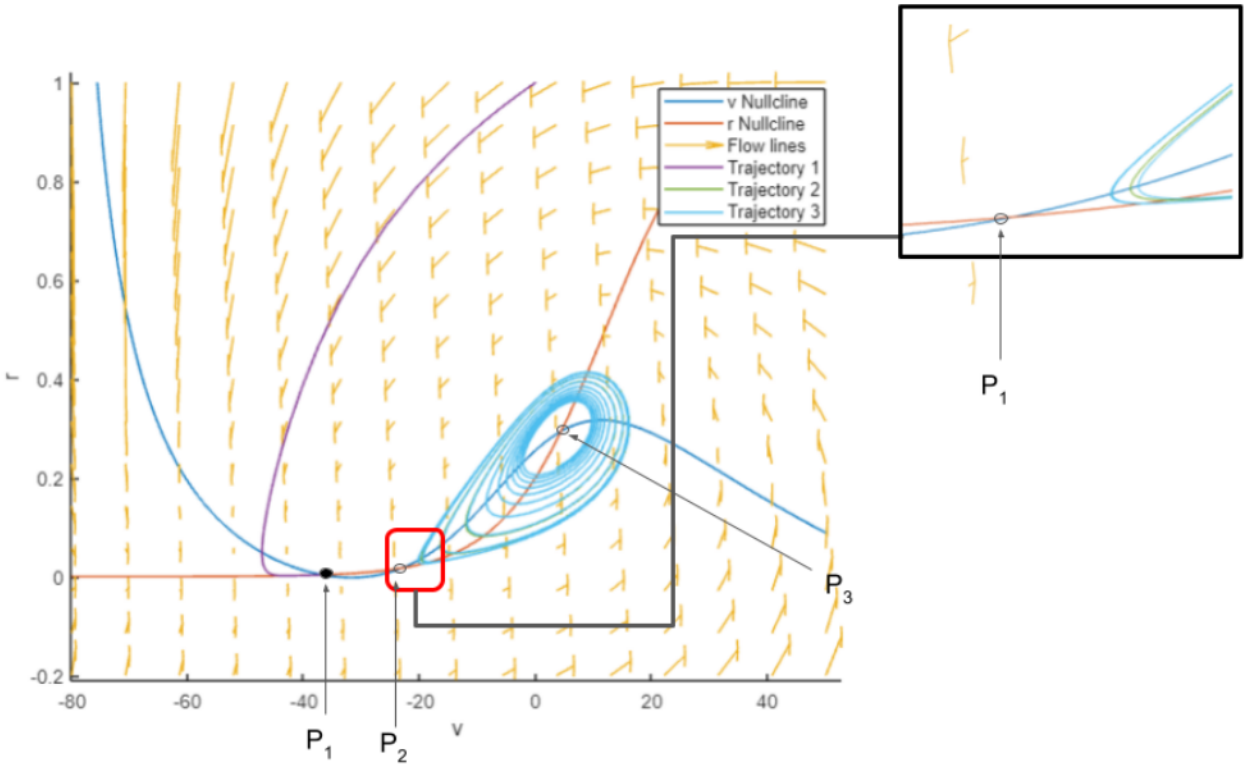

Figure 3.8:
Regime 4: The unstable limit cycle disppears via a subcritical Hopf bifurcation. $F_{coup} = 36$

Table 3.2: Linear stability analysis for Fig 3.8

Point	(v_2^*, r_2^*)	λ_1	λ_2	Type of fixed point
P1	(-36.7944 , 0.0037)	-0.0497	-0.4869	Stable node
P2	(-23.0251 , 0.0175)	0.0741	-0.3167	Saddle
P3	(4.3848 , 0.2941)	0.0005 + 0.3782i	0.0005 - 0.3782i	Unstable Focus

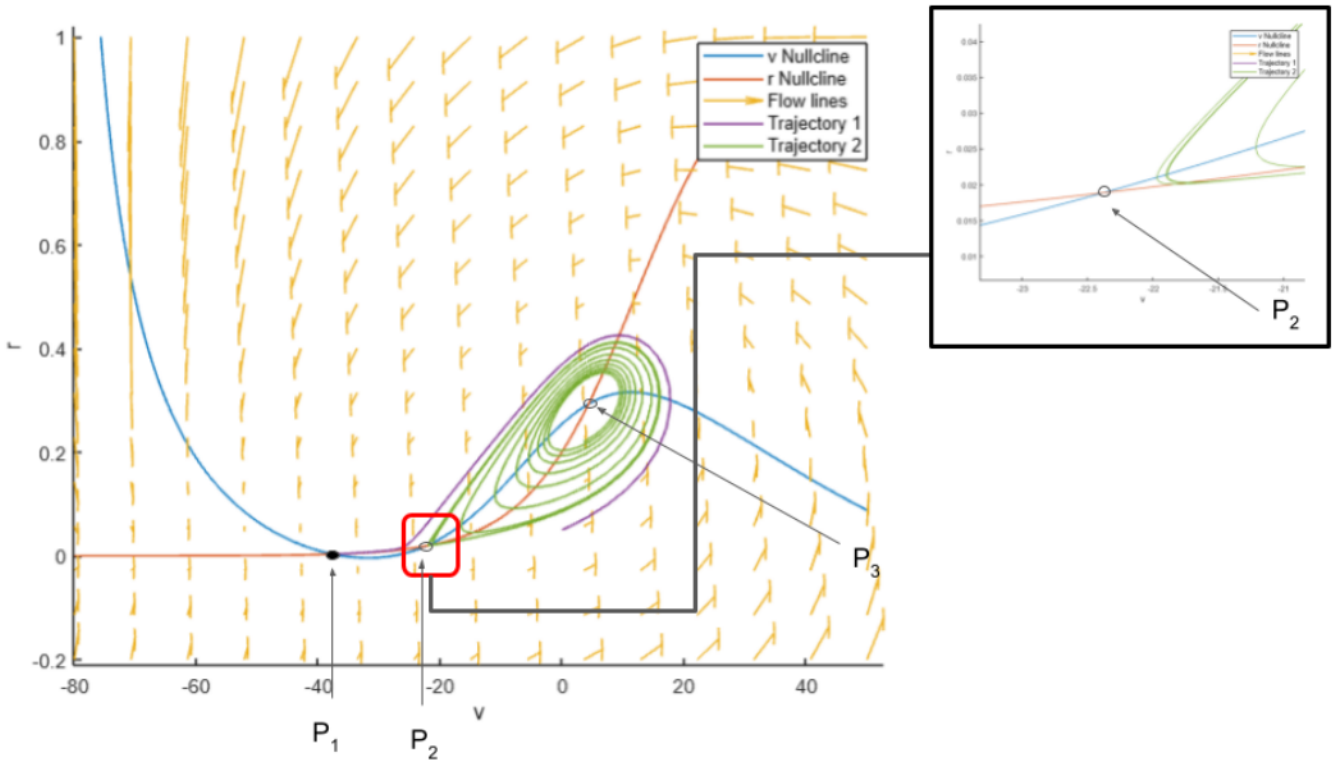

Figure 3.9:
Regime 5: Just before the Stable limit cycle disappears via a homoclinic bifurcation. Here, $F_{coup} = 35.1$

Regime 5: Then, the stable limit cycle touches the saddle P_2 and disappears via a homoclinic bifurcation (Fig 3.9) and Fig 3.10). Now trajectories can only fall into the stable node P_1, and thus the neuron can only show quiescence.

Table 3.3: Linear stability analysis for Fig 3.10

Point	(v_2^*, r_2^*)	λ_1	λ_2	Type of fixed point
P1	(-38.0592 , 0.0032)	-0.0554	-0.5045	Stable node
P2	(-22.1060 , 0.0195)	0.0877	-0.3062	Saddle
P3	(4.2760 0.2916)	0.0025 + 0.3753i	0.0025 - 0.3753i	Unstable Focus

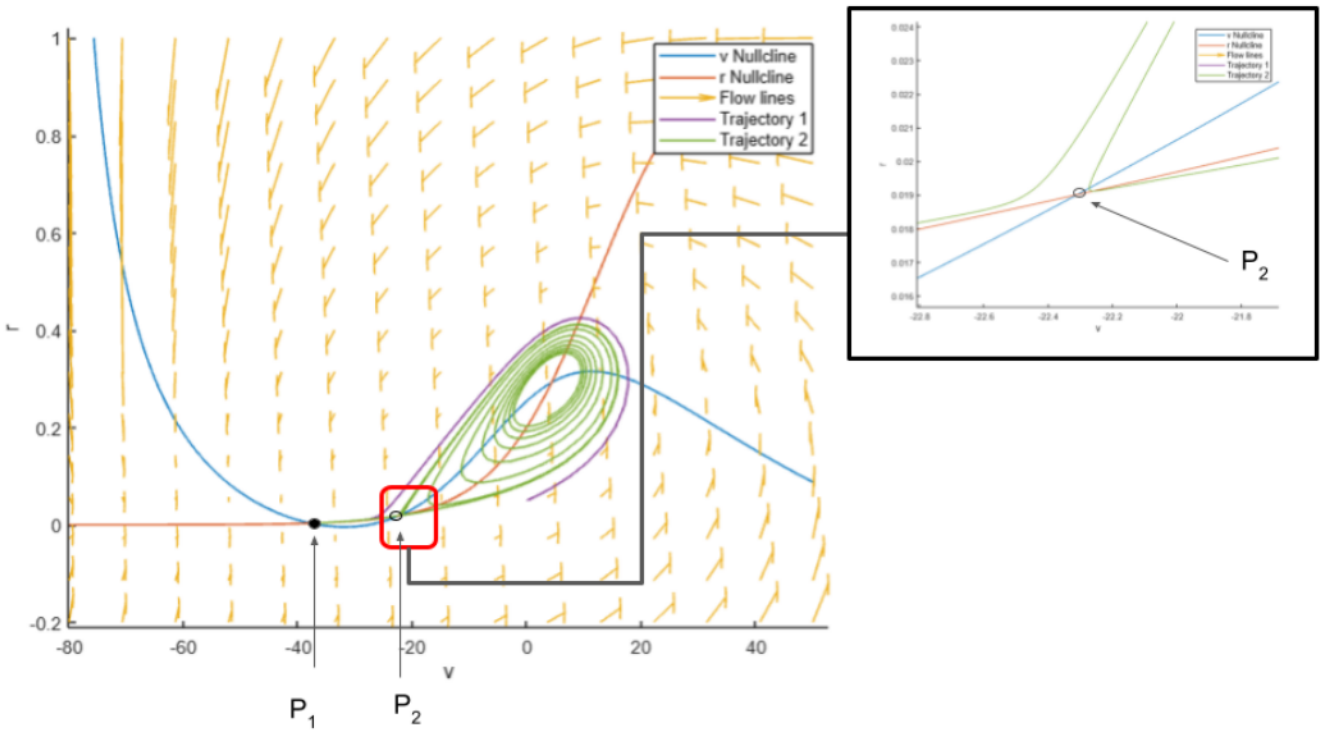

Figure 3.10:
Regime 5: Just after the Stable limit cycle disappears via a homoclinic bifurcation. Here, $F_{coup} = 35$

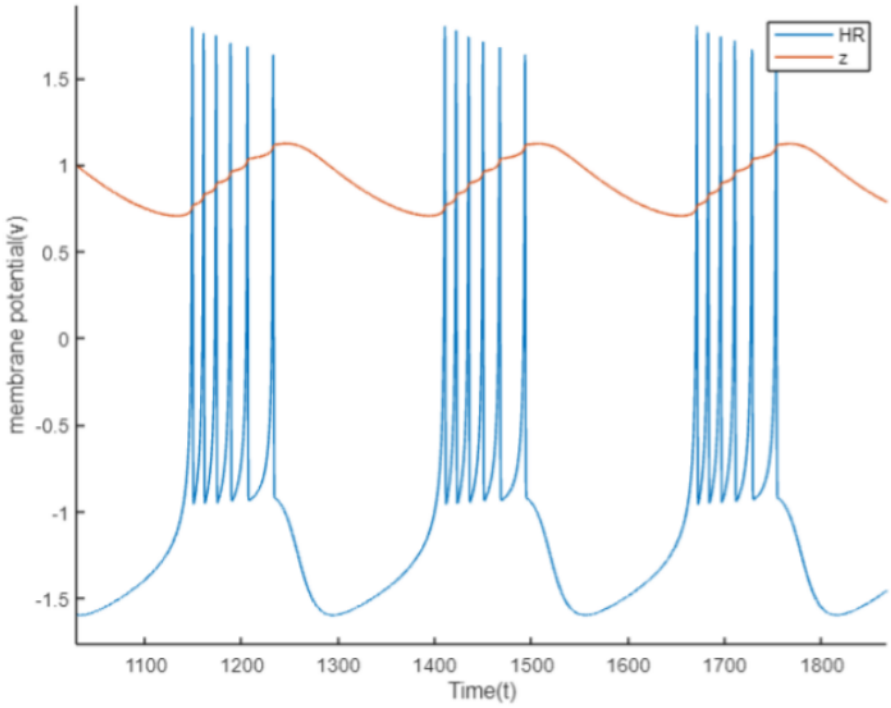

Figure 3.11:
Case 1: Burst in the HR neuron. The plot of the slow variable z has also been shown

3.2.4 Some interesting bursts of the HR neuron as found in extant literature:

The Hindmarsh-Rose neuron is a fast-slow system, where the 3rd variable, i.e. z serves as the slow variable [8]. So we may Consider the first two equations in 2.7 as the fast subsystem, which is modulated by the 3rd variable z. Considering z as a bifurcation parameter, we talk about the bifurcations in the fast subsystem and hold them responsible for the bursting activities obtained, as described below:

Case 1: Parameters taken from Shilnikov et al [8]

Here, the mechanism can be labelled Fold/hom, as the burst starts with a Saddle-node bifurcation where a stable node collides with a saddle and the system loses stability to follow a limit cycle. The burst ends when the limit cycle collides with the saddle and disappears (Fig 3.12).

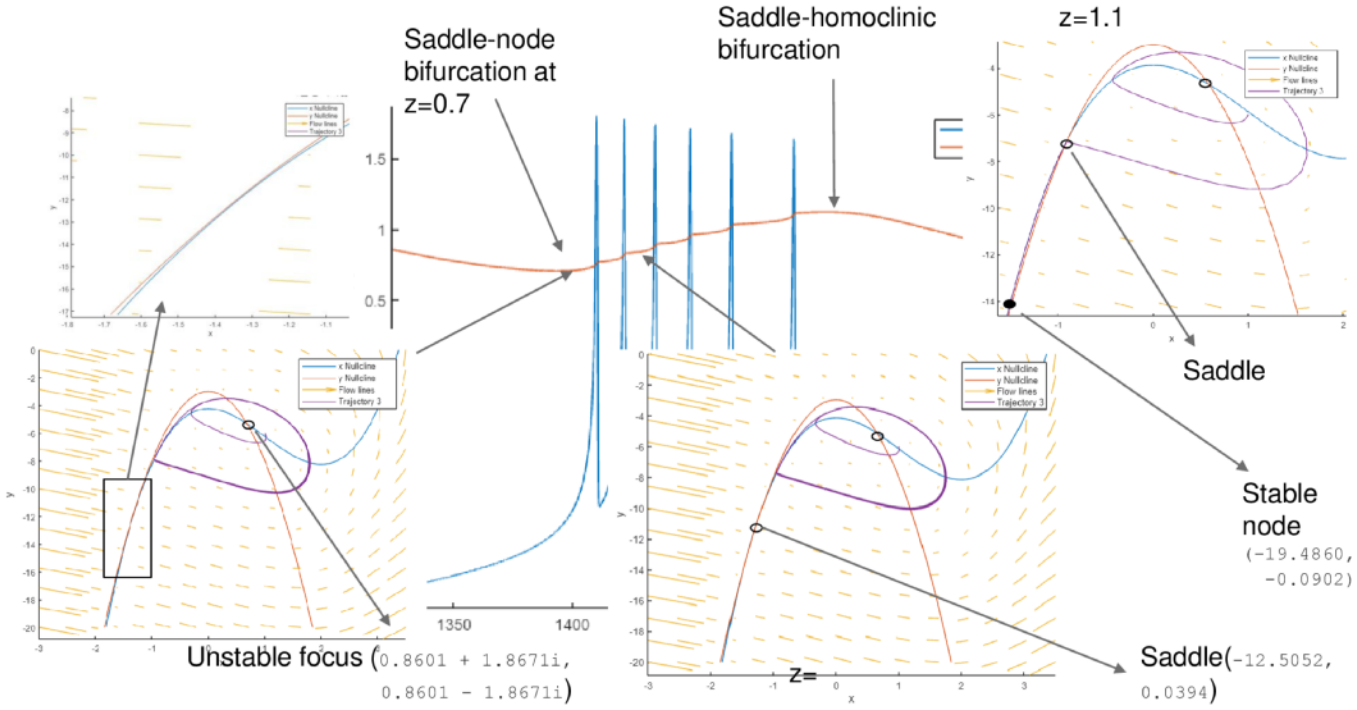

Figure 3.12: Mechanism of the burst in case 1

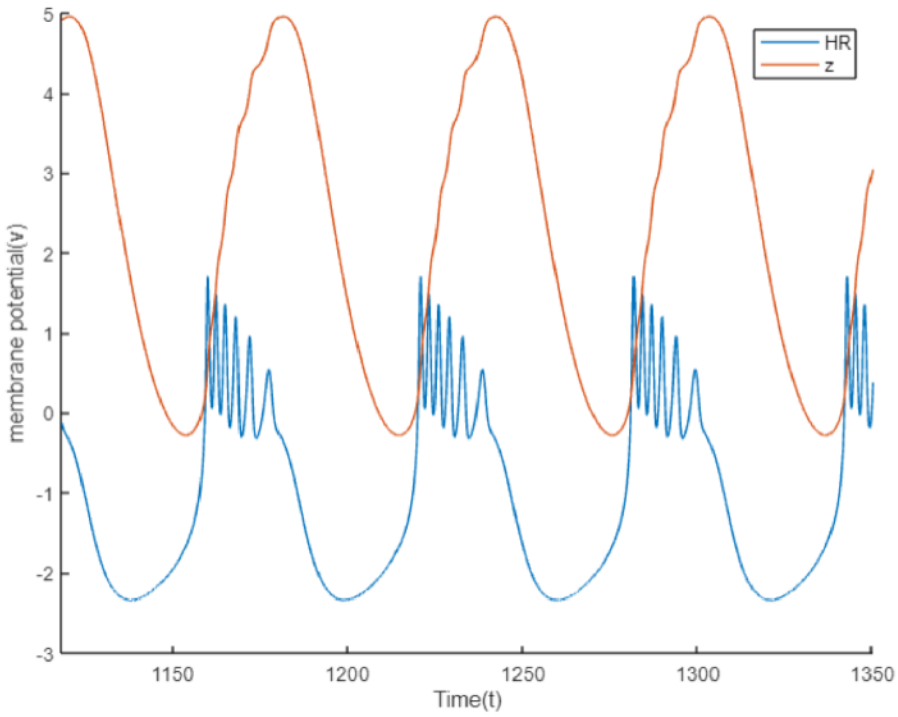

Figure 3.13:
Case 2: Burst in the HR neuron. The plot of the slow variable z has also been shown

Case 2: Parameters taken from Barrio et al [10]

Here, the mechanism can be labelled hopf/hopf, as the burst starts with a supercritical hopf bifurcation at z=1 where a stable limit cycle emerges from a stable focus, the stable focus becomes an unstable focus and the system loses stability to follow the emerged limit cycle. The burst ends by another supercritical bifurcation at z=4.7 when the limit cycle shrinks to the unstable focus and disappears, rendering the unstable focus stable (Fig 3.14 and Fig 3.15).

Case 3: Parameters taken from Corson et al [9]

Here, the mechanism can be labelled fold/hom, as the burst starts with a Saddle-node bifurcation where a stable node collides with a saddle and the system loses stability to follow a limit cycle. The burst ends when the limit cycle collides with the saddle and disappears (Fig 3.17).

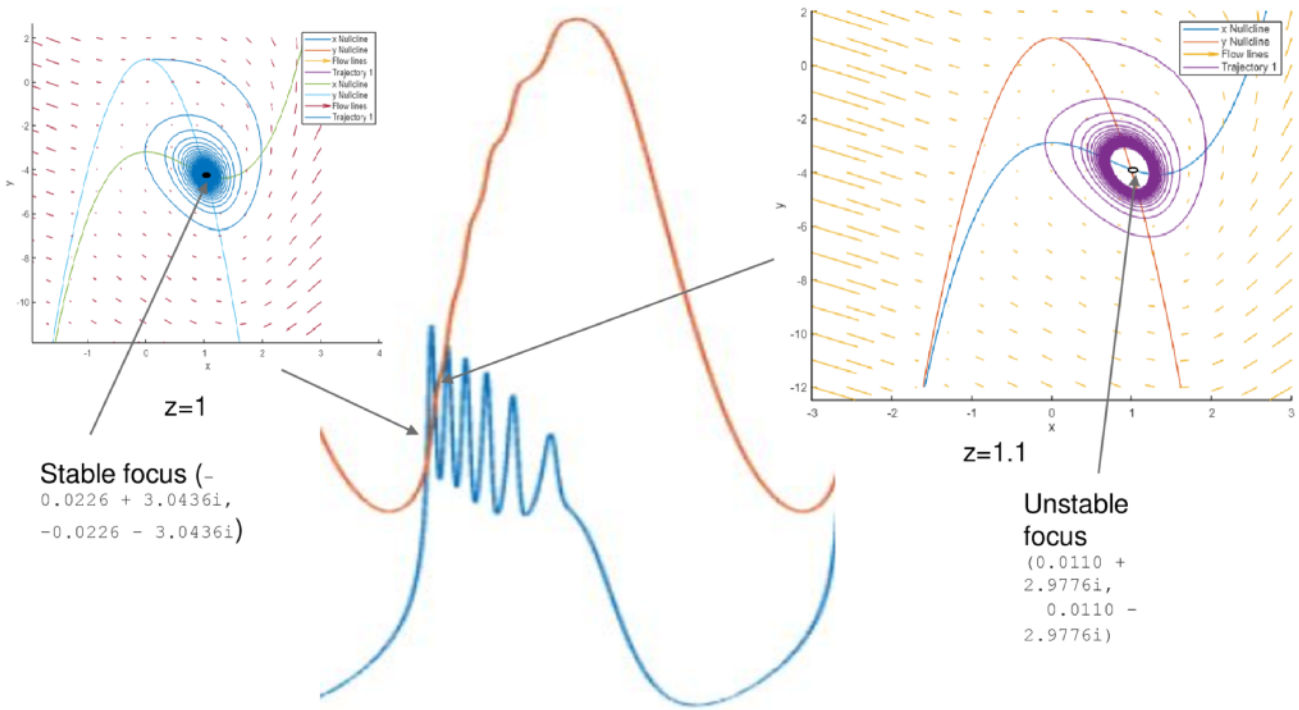

Figure 3.14: Mechanism of the burst in case 2: Start of the burst

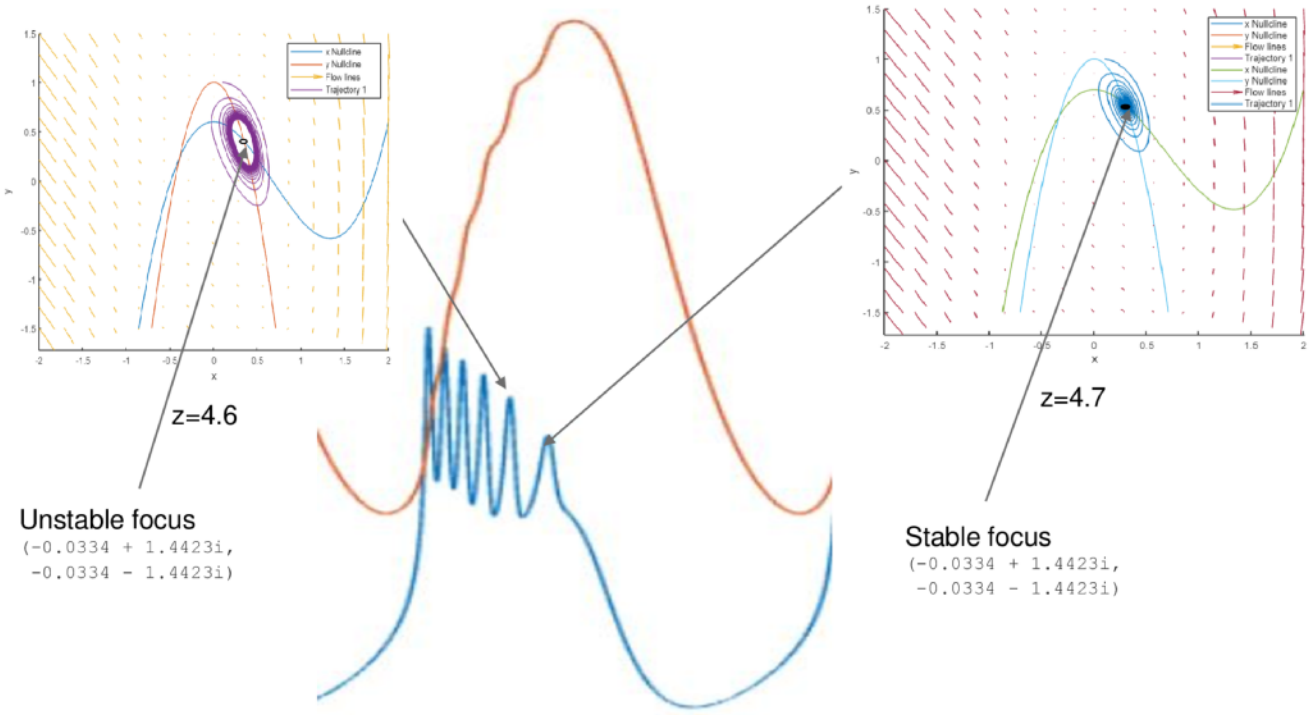

Figure 3.15: Mechanism of the burst in case 2: End of the burst

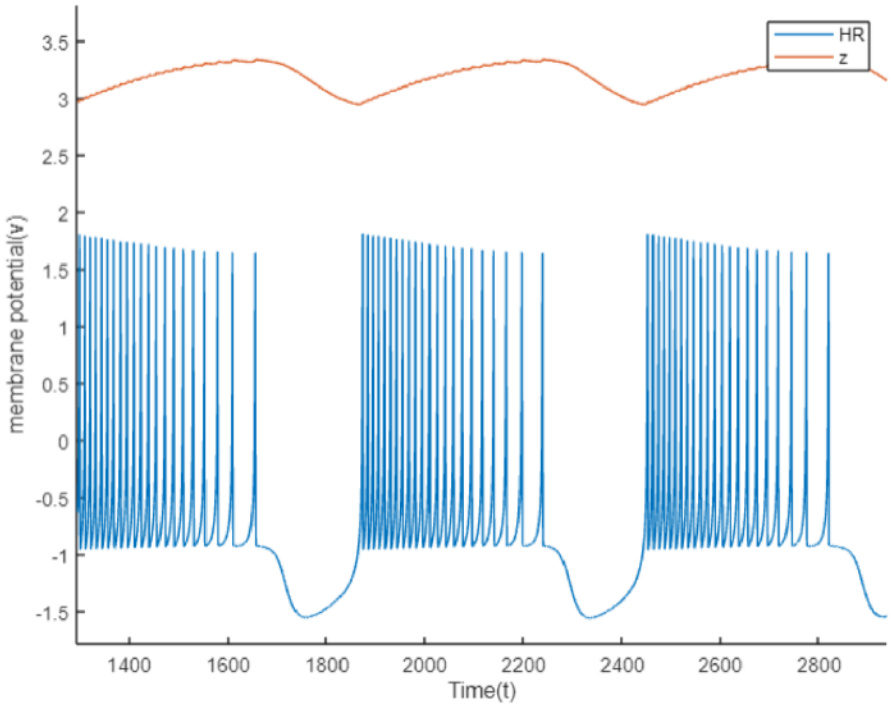

Figure 3.16:
Case 3: Burst in the HR neuron. The plot of the slow variable z has also been shown

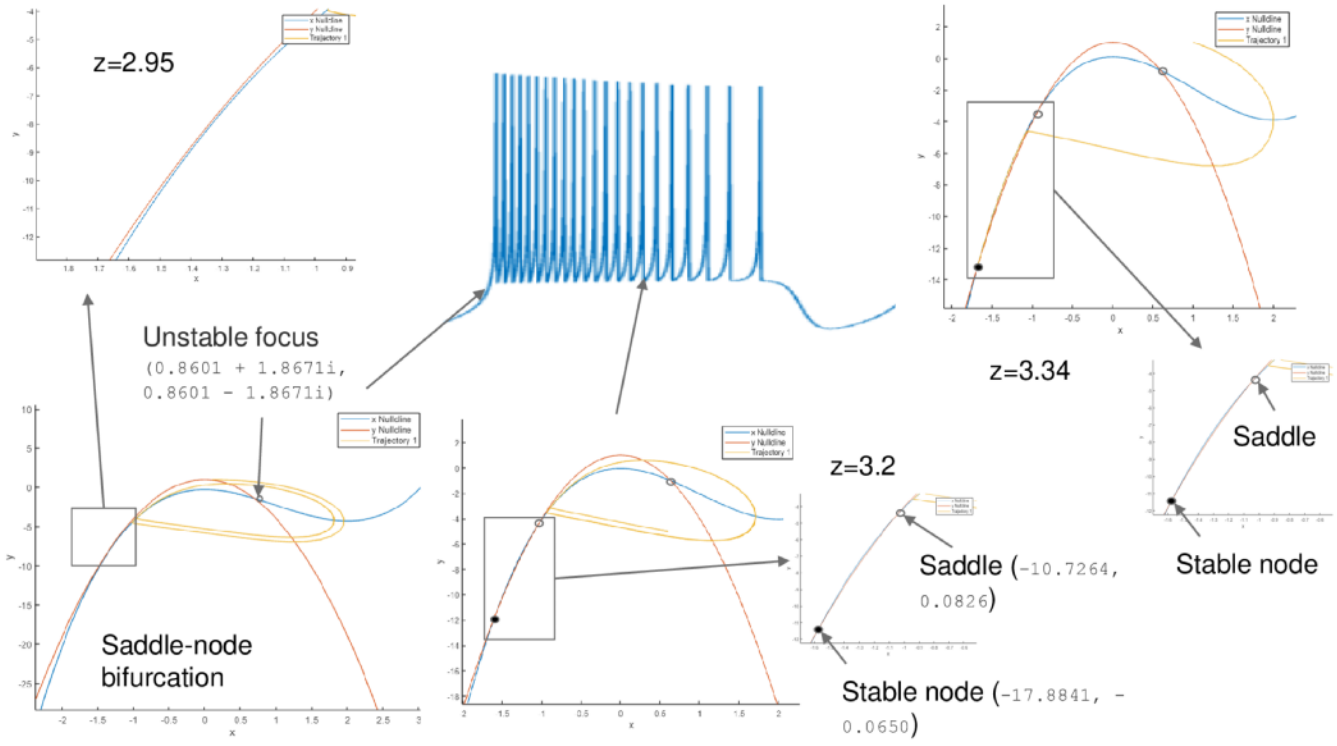

Figure 3.17: Mechanism of the burst in case 3

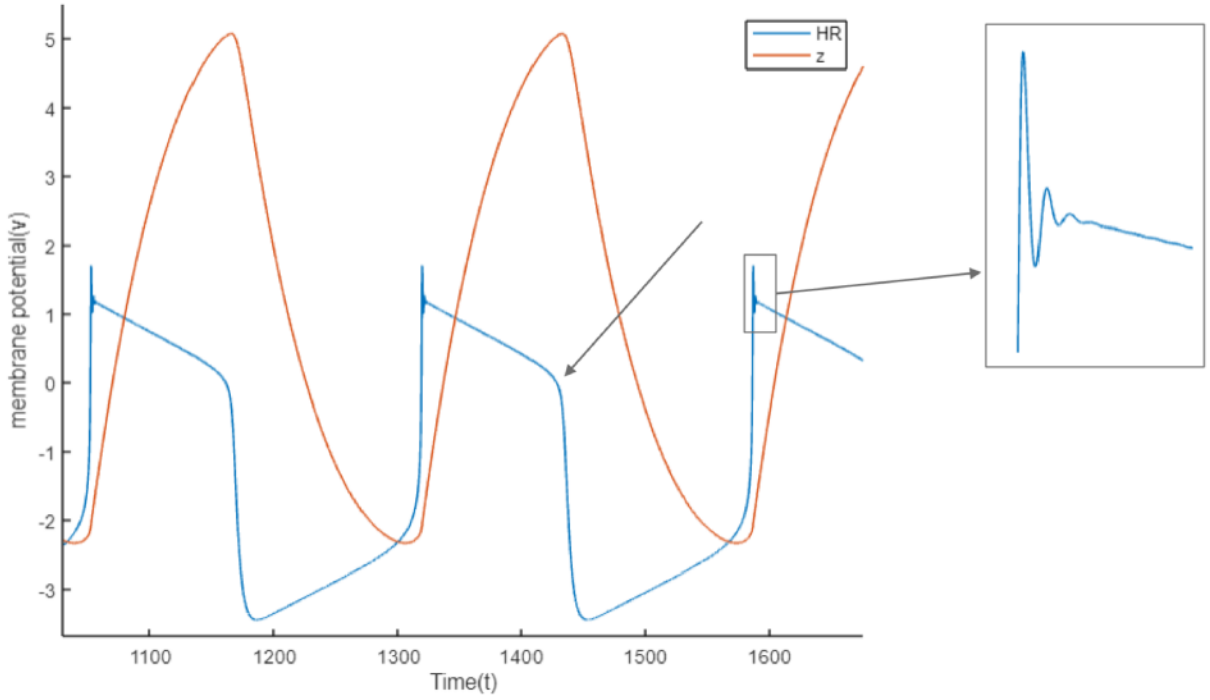

Figure 3.18:
Case 4: Burst in the HR neuron. The plot of the slow variable z has also been shown

Case 4: Parameters taken from Storace et al [12]

Here, the mechanism can be labelled Fold/fold, as the burst starts with a Saddle-node bifurcation at z=1.9 where a stable node collides with a saddle and the system loses stability to follow a spiralling trajectory to the stable focus. However, before the trajectory reaches the focus, the focus becomes a stable node and collides with the saddle that emerged in the previous bifurcation, and the system goes to the stable node that emerged in the previous bifurcation, thus ending the burst (Fig 3.19).

Case 5: Parameters taken from Innocenti et al [11]

Here, the mechanism can be labelled Fold/hom, as the burst starts with a Saddle-node bifurcation where a stable node collides with a saddle and the system loses stability to follow a limit cycle. The burst ends when the limit cycle collides with the saddle and disappears (Fig 3.21).

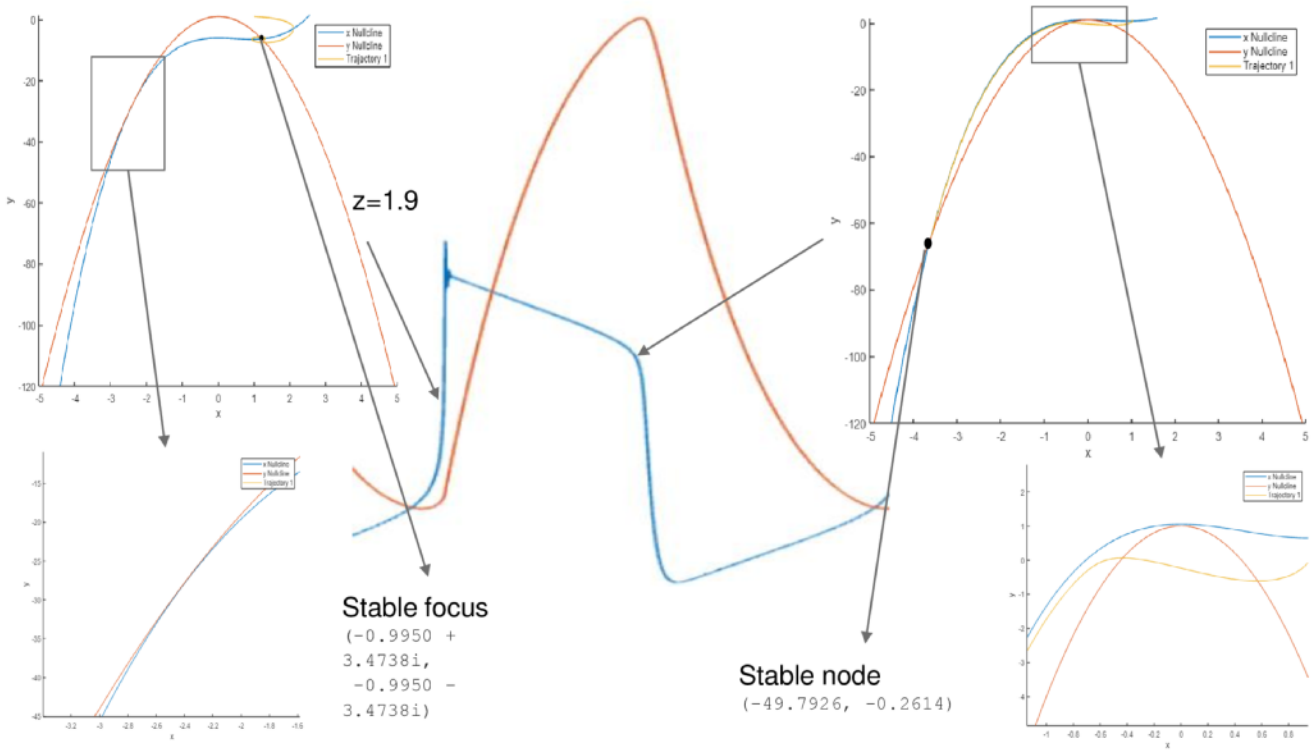

Figure 3.19: Mechanism of the burst in case 4

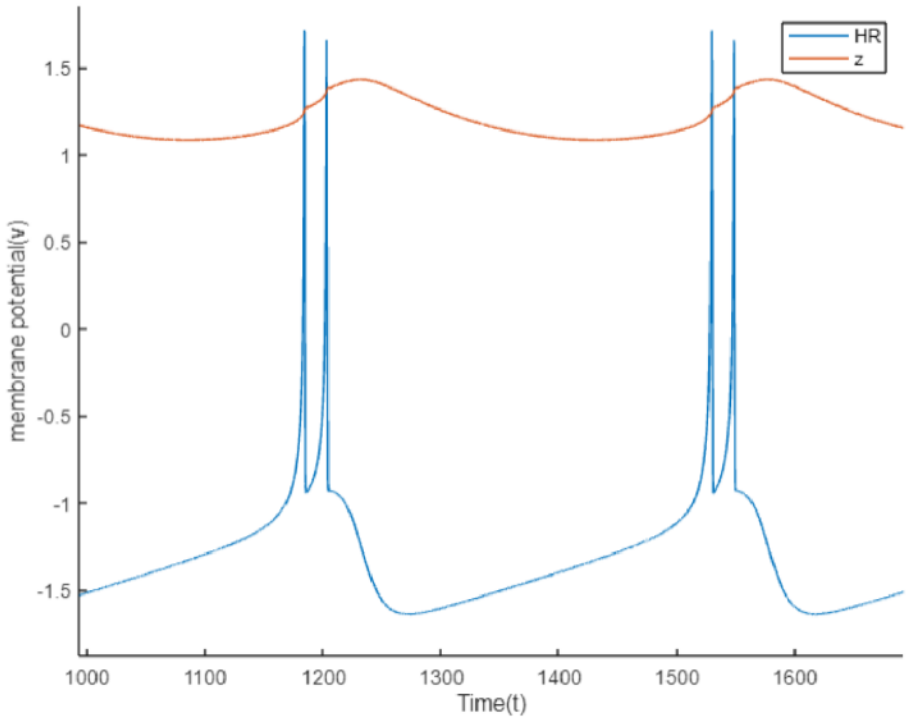

Figure 3.20:
Case 5: Burst in the HR neuron. The plot of the slow variable z has also been shown

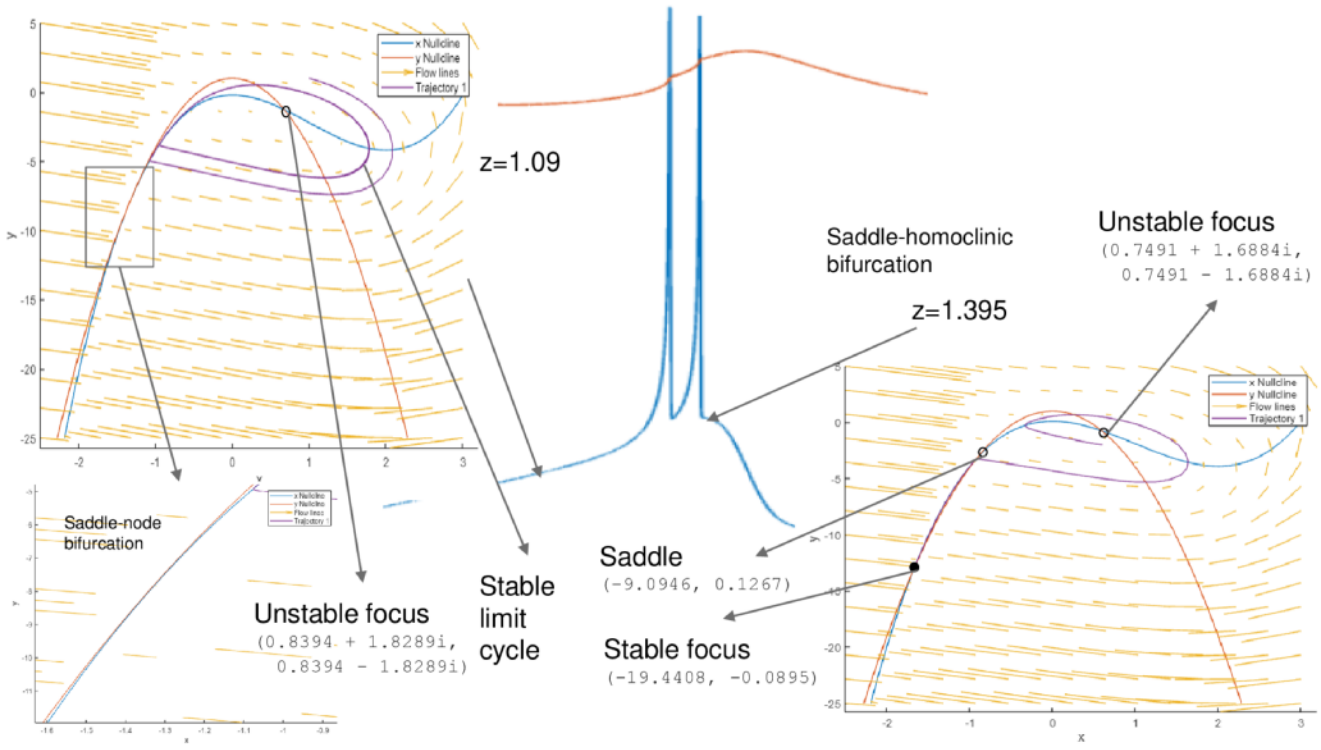

Figure 3.21: Mechanism of the burst in case 5

Chapter 4

Results and Discussions

4.1 Unidirectional Case

In this section, we report some observations obtained by coupling the HR neuron unidirectionally to the ML neuron in cases 1-10, as in (3.1). And then we report a peculiar case where the ML neuron is driving the HR neuron. The parameters of the type I and II ML neurons are taken from [7] and those of the HR neurons from [8] , [10], [9], [11] and [12].

Case 1:

Paper used for HR neuron parameters: Shilnikov et al [8]
The parameters: $I = 5; a = 1; b = 3; c = -3; d = 5; r = 0.002; s = 4; x_R = -1.3;$
ML neuron type: Type II

The time series plot of the HR neuron and that of the ML neuron is shown together in Fig (4.1). In this case the coupling constant $\gamma = 10$. The mechanism of the burst in the ML neuron is illustrated in Fig 4.2. This mechanism relies on the method described in 3.5. Here we look at the values of F_{coup} at different stages of the ML burst and feed the same value into (3.5) and subsequently look at the respective nullclines and phase portraits. On doing this, we observe that the burst starts as a pair of stable and unstable limit cycles

Table 4.1: Linear stability analysis for P around $t = 1100$

time Type	F_{coup}	(v_2^*, r_2^*)	λ_1	λ_2
1100 Stable focus	113	(9.1182, 0.4179)	-0.0994 + 0.4723i	-0.0994 - 0.4723i
1101 Stable focus	112	(9.0685 , 0.4166)	-0.0983 + 0.4717i	-0.0983 - 0.4717i
1103 Stable focus	111	(9.0187 0.4152)	-0.0972 + 0.4710i	-0.0972 - 0.4710i
1104 Stable focus	110	(8.9687 , 0.4138)	-0.0961 + 0.4703i	-0.0961 - 0.4703i

appear (Fig 3.4) and the ML neuron can now operate in that limit cycle and show spikes. Around $t = 1152$, a saddle-node bifurcation occurs. Around $t = 1229$, there is a peculiar change in the shape of the burst, and this may be attributed to a homoclinic bifurcation occurring around that point, and then the burst stops after showing a single spike. We may say that the last spike is just an excitation that eventually subsides into a quiescent state as the trajectory leads itself to the stable node P_1. So this burst maybe called a complicated kind of fold/hom burst, as a fold bifurcation happens towards the start and a homoclinic one towards the end.

To support this mechanism, we track the natures of the fixed points at the corresponding time points via linear stability analyses. The results from the analyses are shown below in tables:

Around $t = 1100$:

Here, there is only 1 fixed point P. We list its stability against a few nearby values of F_{coup} in Tab 4.1

Around $t = 1152$:

Here, there is one fixed point P. We look at the linear stability analysis in Table 4.2:

Table 4.2: Linear stability analysis for P around $t = 1152$

time Type of fixed point	F_{coup}	(v_2^*, r_2^*)	λ_1	λ_2
1152 Stable focus	63.6	(6.3698, 0.3436)	-0.0393 + 0.4253i	-0.0393 - 0.4253i
1153 Stable focus	60.9	(6.1956, 0.3391)	-0.0357 + 0.4216i	-0.0357 - 0.4216i
1154 Stable focus	57.4	(5.9646, 0.3332)	-0.0308 + 0.4165i	-0.0308 - 0.4165i
1155 Stable focus	53.9	(5.7270, 0.3272)	-0.0260 + 0.4112i	-0.0260 - 0.4112i

Table 4.3: Linear stability analysis for P_3 around $t = 1229$

time Type of fixed point	F_{coup}	(v_2^*, r_2^*)	λ_1	λ_2
1229.12 Unstable focus	34.7	(4.2769, 0.2916)	0.0025 + 0.3753i	0.0025 - 0.3753i
1229.27 Unstable focus	35.0	(4.3019 , 0.2922)	0.0020 + 0.3760i	0.0020 - 0.3760i
1229.41 Unstable focus	35.67	(4.3575, 0.2935)	0.0010 + 0.3775i	0.0010 - 0.3775i
1229.54 Stable focus	36.79	(4.4495, 0.2957)	-0.0007 + 0.3799i	-0.0007 - 0.3799i

Around $t = 1229$:

Here, There are 3 fixed points: P_1, P_2 and P_3: We look at them in tables 4.3, 4.4 and 4.5.

Case 2:

Paper used for HR neuron parameters: Shilnikov et al [8]

ML neuron type: Type I

Table 4.4: Linear stability analysis for P_1 around $t = 1229$

time	F_{coup}	(v_2^*, r_2^*)	λ_1	λ_2
Type of fixed point				
1229.12	34.7	(-38.0500, 0.0032)	-0.0554	-0.5043
Stable node				
1229.27	35.0	(-37.7721 , 0.0033)	-0.0542	-0.5004
Stable node				
1229.41	35.67	(-37.1267, 0.0035)	-0.0513	-0.4914
Stable node				
1229.54	36.79	(-35.9497 , 0.0040)	-0.0455	-0.4754
Stable node				

Table 4.5: Linear stability analysis for P_2 around $t = 1229$

time	F_{coup}	(v_2^*, r_2^*)	λ_1	λ_2
Type of fixed point				
1229.12	34.7	(-22.1125, 0.0194)	0.0876	-0.3063
Saddle				
1229.27	35.0	(-22.3112, 0.0190)	0.0846	-0.3085
Saddle				
1229.41	35.67	(-22.7797, 0.0180)	0.0776	-0.3139
Saddle				
1229.54	36.79	(-23.6618, 0.0163)	0.0651	-0.3240
Saddle				

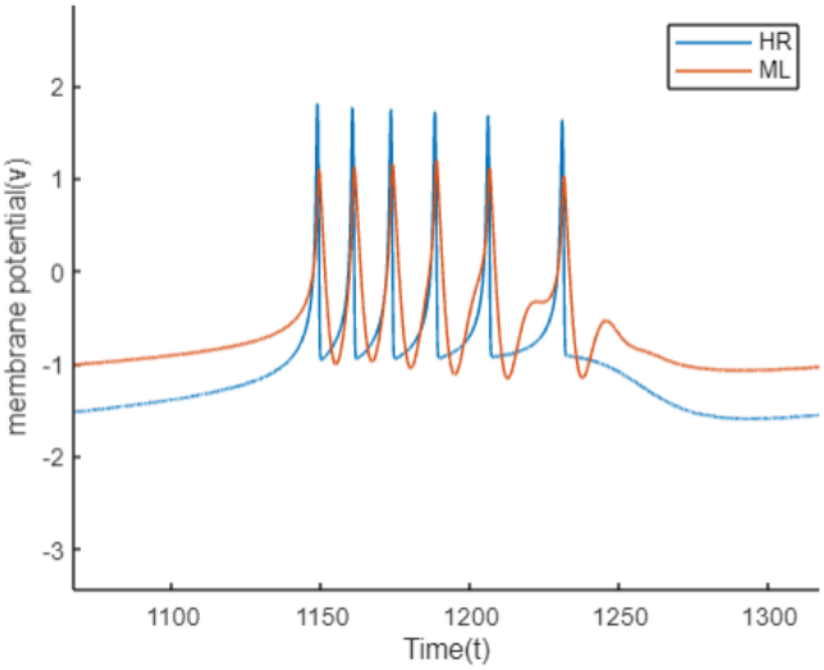

Figure 4.1: Time series plot of the HR and ML neurons together in Case 1

Case 3:

Paper used for HR neuron parameters: Barrio et al [10]
The parameters: $I = 4; a = 1; b = 2; c = 1; d = 5; r = 0.05; s = 4; x_R = -8/5;$ **ML neuron type:** Type I

The time series plot of both the neurons is shown in Fig 4.4. In this case the coupling constant $\gamma = 10$.

Case 4:

Paper used for HR neuron parameters: Corson et al [9]
The parameters: $I = 3.25; a = 1; b = 3; c = 1; d = 5; r = 0.001; s = 4; x_R = -(\sqrt{5}+1)/2;$ **ML neuron type:** Type I

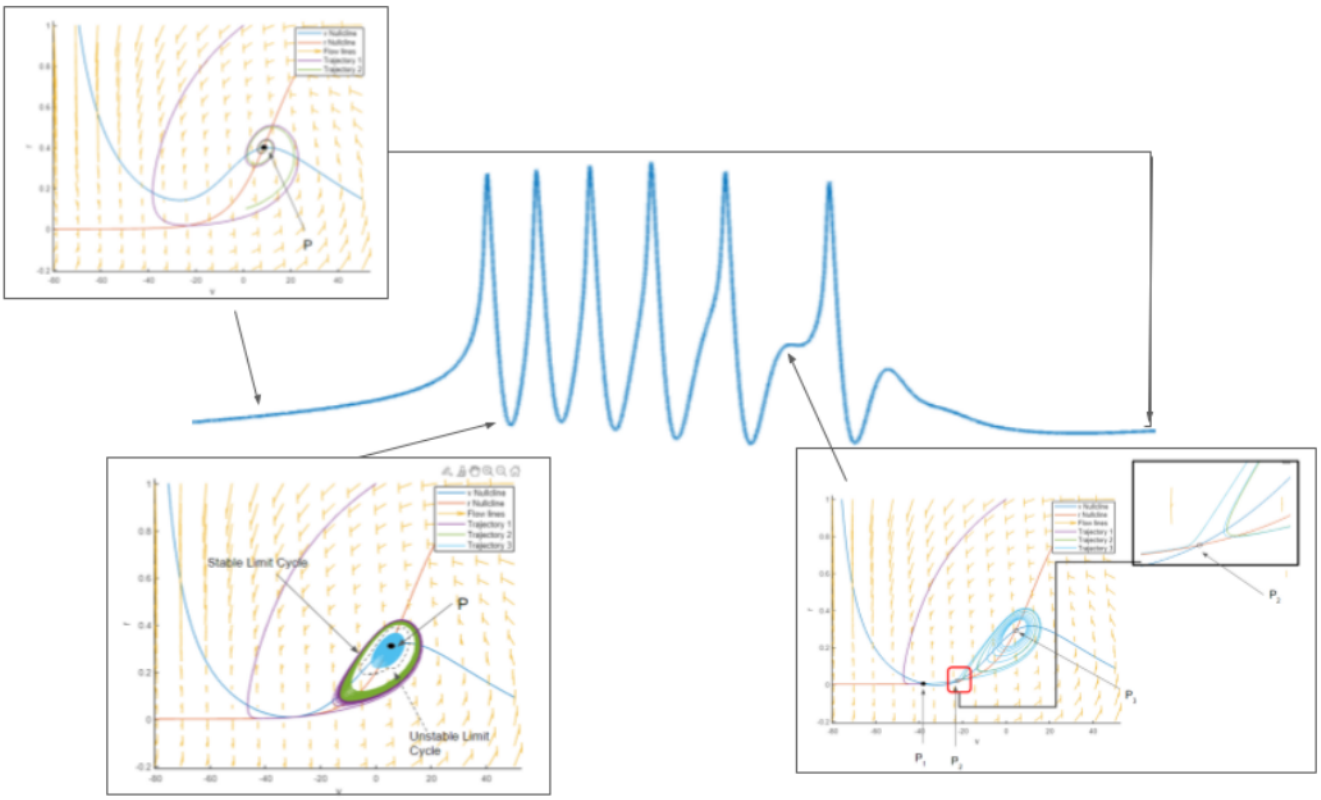

Figure 4.2: Mechanism of the Burst in case 1

The time series plot of both the neurons is shown in Fig 4.3. In this case the coupling constant $\gamma = 10$.

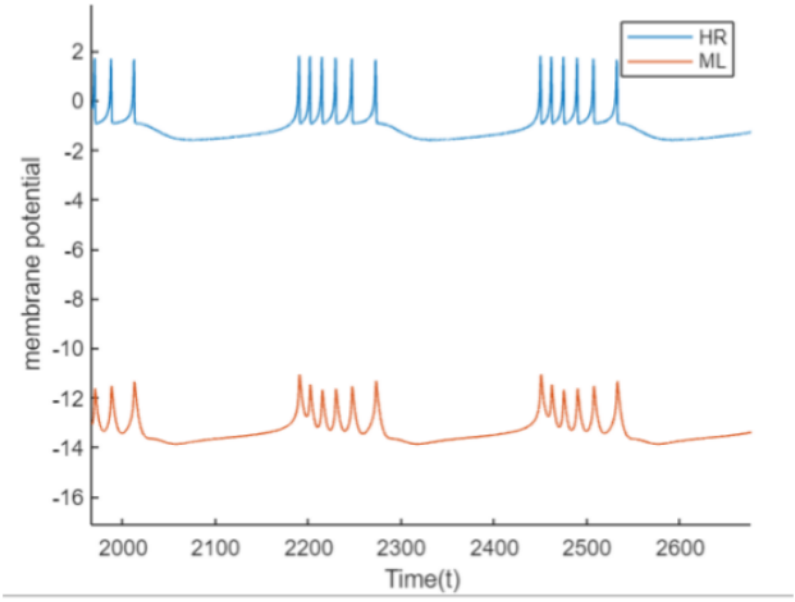

Figure 4.3: Time series plot of the HR and ML neurons for case 2

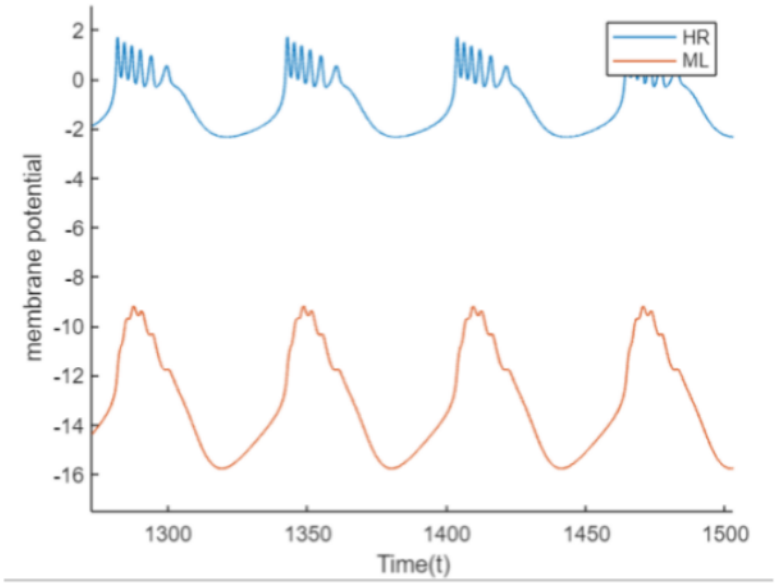

Figure 4.4: Time series plot of the HR and ML neurons for case 3

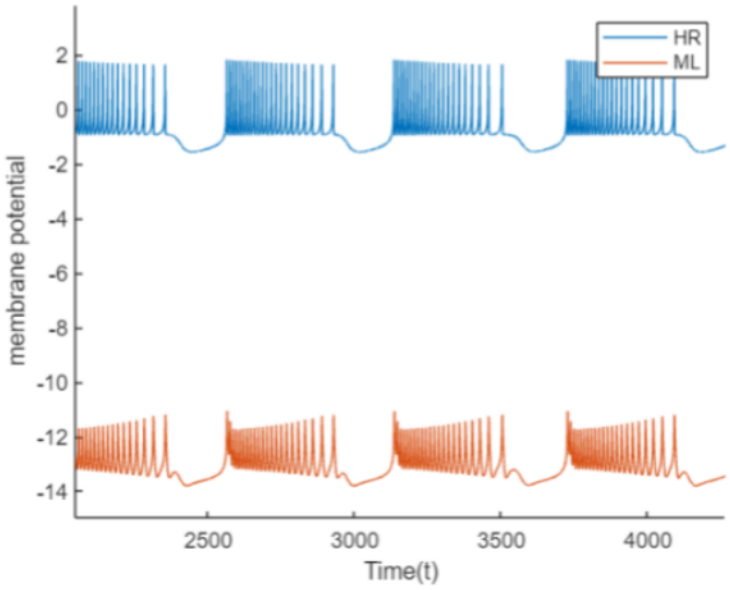

Figure 4.5: Time series plot of the HR and ML neurons for case 4

The time series plot of both the neurons is shown in Fig 4.5. In this case the coupling constant $\gamma = 10$.

Case 5:

Paper used for HR neuron parameters: Storace et al [12]
Parameters: $I = 4; a = 1; b = 1.4; c = 1; d = 5; r = 0.01; s = 4; x_R = -1.6$; **ML neuron type:** Type I

The time series plot of both the neurons is shown in Fig 4.6. In this case the coupling constant $\gamma = 10$.

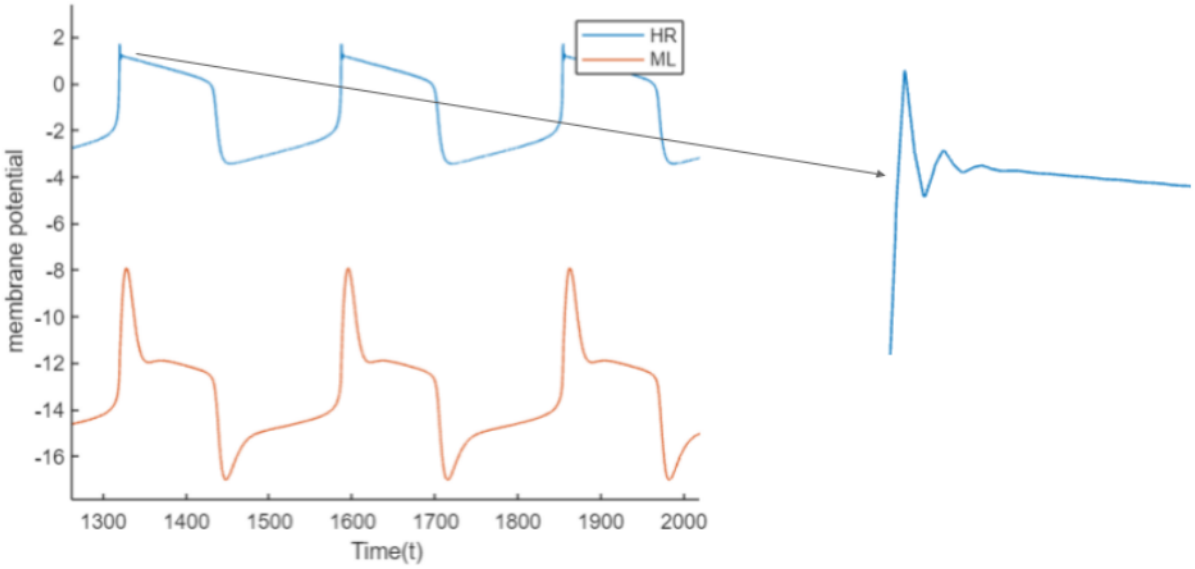

Figure 4.6: Time series plot of the HR and ML neurons for case 5

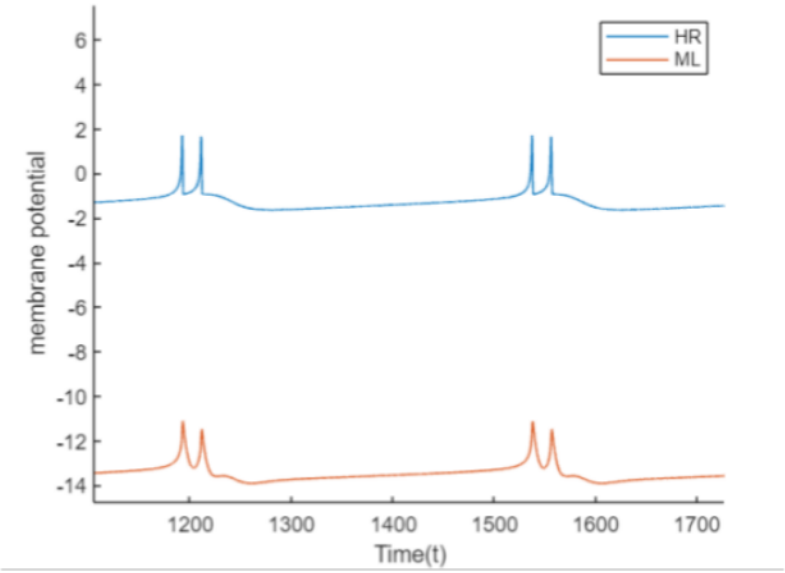

Figure 4.7: Time series plot of the HR and ML neurons for case 6

Case 6:

Paper used for HR neuron parameters: Innocenti et al [11]
Parameters: $I = 1.3; a = 1; b = 3; c = 1; d = 5; r = 0.0021; s = 4; x_R = -1.6$; **ML neuron type:** Type I

The time series plot of both the neurons is shown in Fig 4.7. In this case the coupling constant $\gamma = 10$.

Case 7:

Paper used for HR neuron parameters: Barrio et al [10]
ML neuron type: Type II

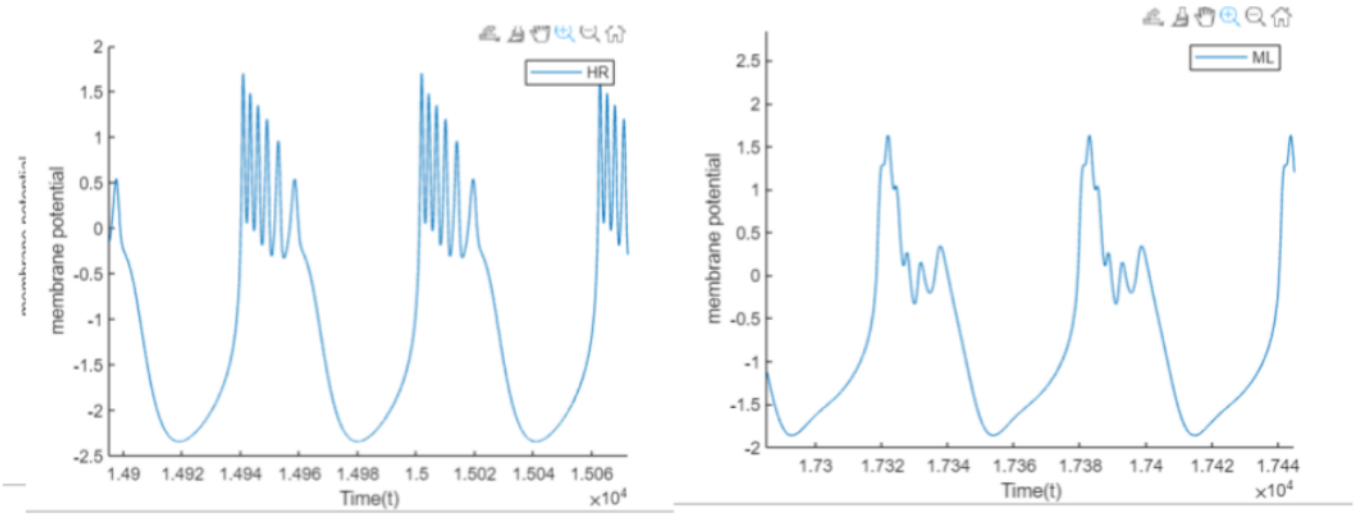

Figure 4.8: Time series plot of the HR and ML neurons for case 7

The time series plot of both the neurons is shown in Fig 4.8. In this case the coupling constant $\gamma = 10$.

Case 9:

Paper used for HR neuron parameters: Storace et al [11]
ML neuron type: Type II

The time series plot of both the neurons is shown in Fig 4.10. In this case the coupling constant $\gamma = 10$.

Case 8:

Paper used for HR neuron parameters: Corson et al [9]
ML neuron type: Type II

The time series plot of both the neurons is shown in Fig 4.9. In this case the coupling constant $\gamma = 10$.

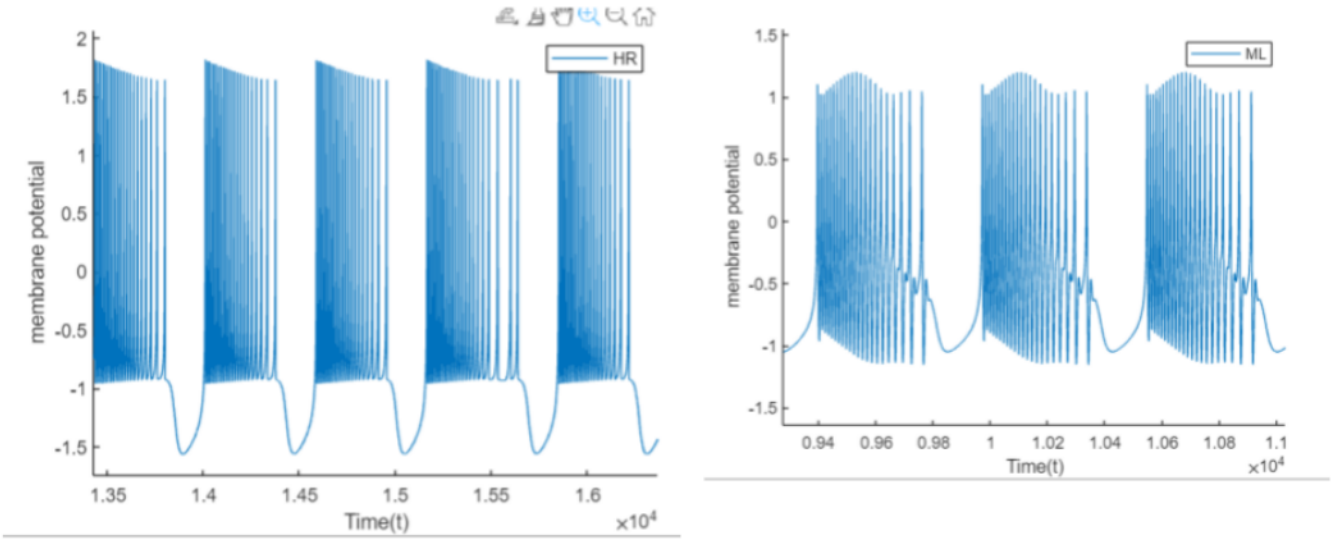

Figure 4.9: Time series plot of the HR and ML neurons for case 8

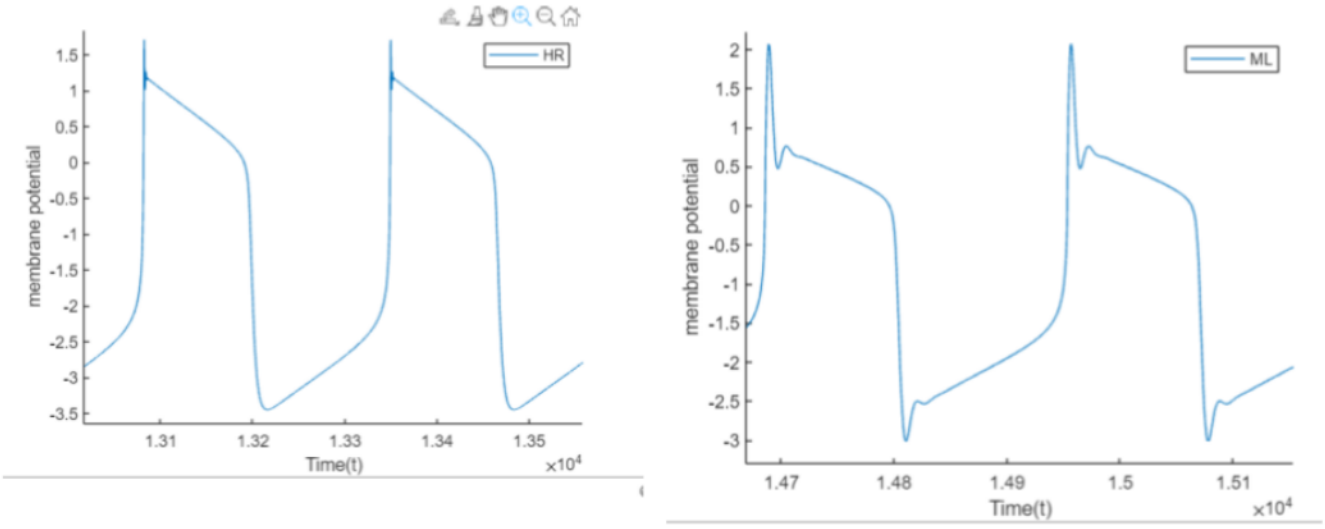

Figure 4.10: Time series plot of the HR and ML neurons for case 9

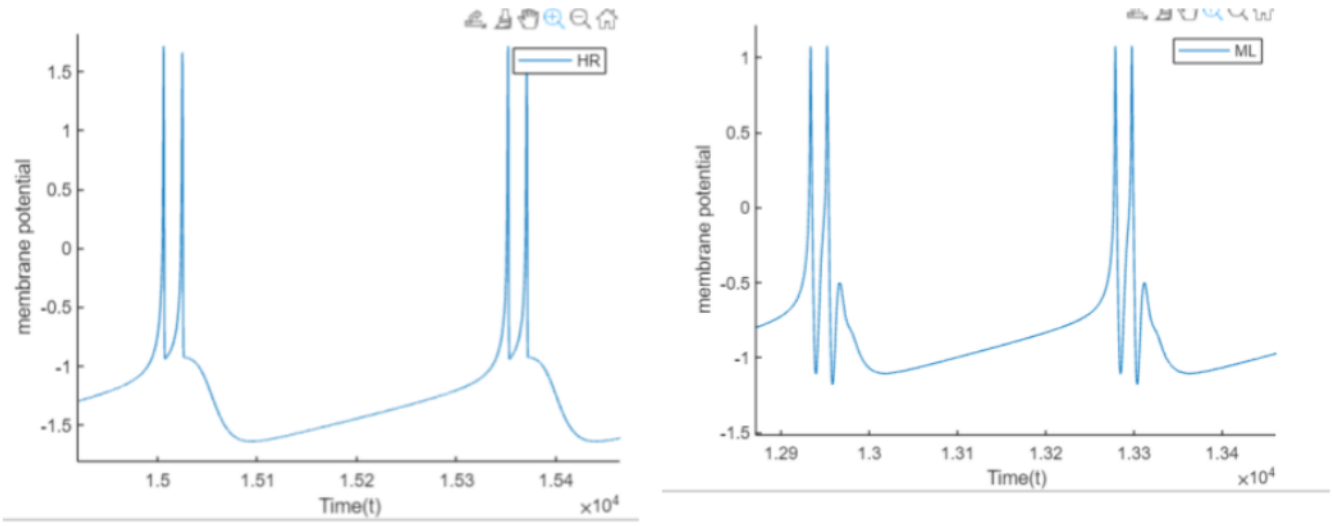

Figure 4.11: Time series plot of the HR and ML neurons for case 10

Case 10:

Paper used for HR neuron parameters: Innocenti et al [12]
ML neuron type: Type II

The time series plot of both the neurons is shown in Fig 4.11. In this case the coupling constant $\gamma = 10$.

Case 11:

We observe another peculiar case with the parameter set $C = 5; g_L = 2; g_{Ca} = 4; g_K = 8; V_L = -60; V_{Ca} = 120; V_K = -80; V_1 = -1.2; V_2 = 18; V_3 = 12; V_4 = 17.4; \phi = 1/3; I = 2; a = 1; b = 3; c = 1; d = 5; r = 0.001; s = 4; x_R = -8/5;$

This is a regime where the HR neuron (driver) is bursting. We list some observations

about the ML neuron (driven one): Quiescent at $\gamma = 0$ (i.e. the uncoupled case). Bursting amplitude grows with γ. Between $\gamma = 1.6$ and $\gamma = 1.7$, strange aperiodic behavior happens (seems like there is no pattern in the spiking amplitude). Intermittent periodic and aperiodic behavior between $\gamma = 5$ to $\gamma = 7$. Then the phenomenon of bursting reappears at $\gamma = 10$, with a somewhat strange pattern.

Case 12: ML neuron driving HR neuron unidirectionally

In this case, a type-I ML neuron drives an HR neuron with parameters from [8] unidirectionally, while both the neurons receive the same external stimulus current I. i.e. the equations are:

$$\begin{aligned} \dot{v_1} &= -av_1^3 + bv_1^2 + y - z + \gamma(v_2 - v_1) + I \\ \dot{y} &= -dv_1^2 + c - y \\ \dot{z} &= r[s(v_1 - x_R) - z] \\ C\dot{v_2} &= -g_L(v_2 - V_L) - g_K r(v_2 - V_K) - g_{Ca} m_\infty (v_2 - V_{Ca}) + I \\ \dot{r} &= \lambda(v_2)(r_\infty - r) \end{aligned} \tag{4.1}$$

We set $I = 40$. The uncoupled (with $\gamma = 0$) system is shown in Fig 4.16 and the coupled one (with $\gamma = 10$) in Fig 4.17.

In the uncoupled scenario, both the neurons are showing tonic spiking. After coupling, the HR neuron bursts with a frequency (frequency of occurrence of bursts) same as the frequency of the driving ML neuron.

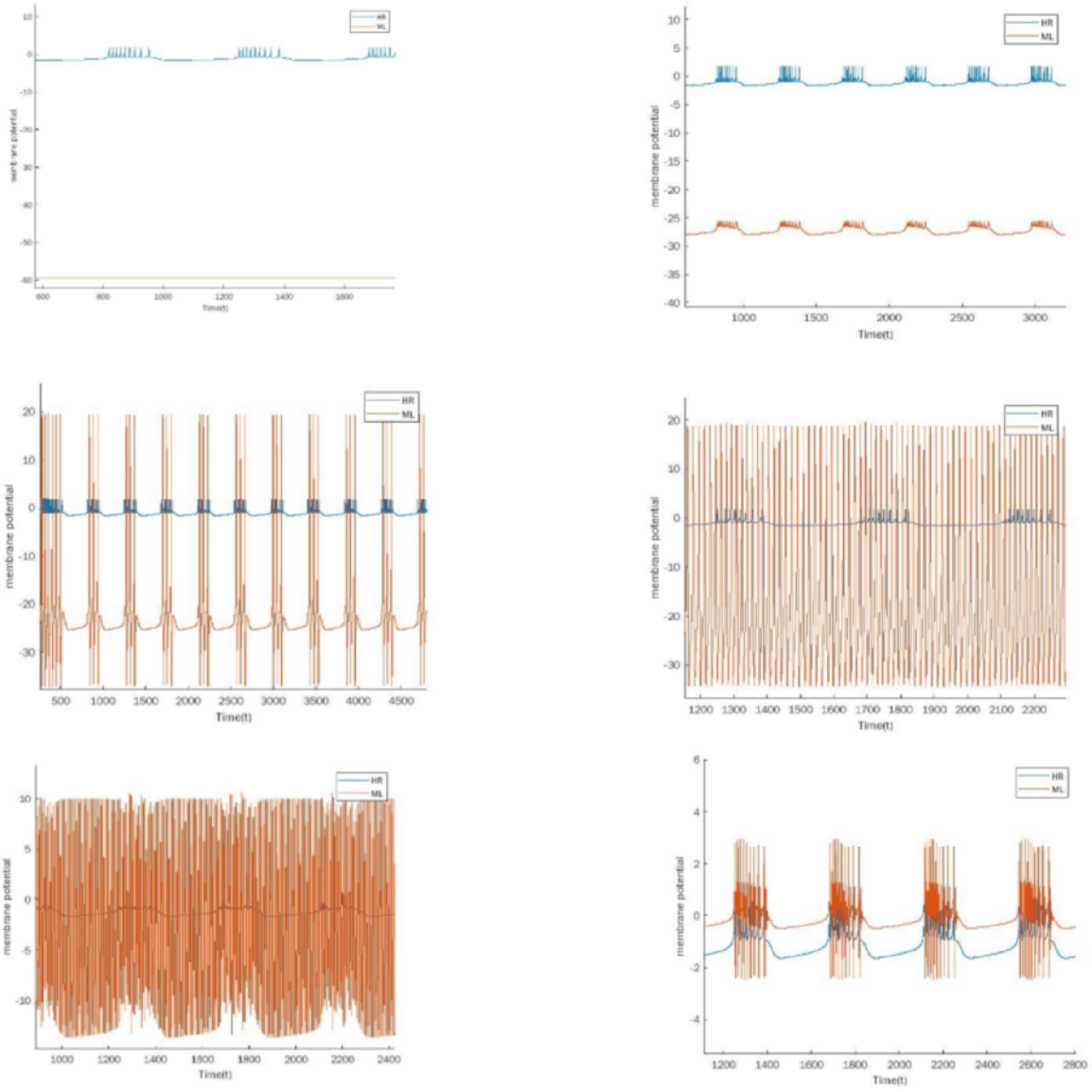

Figure 4.12:
In the unidirectionally coupled system, we observe a bursting ML neuron at low γ. Starting from $\gamma = 0$, the amplitude of the bursting oscillations keep rising from 0. At around $\gamma = 1.6$, the bursting turns into periodic spiking of aperiodic amplitudes. This subsides to bursting again at around $\gamma = 9$. With parameter values $C = 5$; $g_L = 2$; $g_{Ca} = 4$; $g_K = 8$; $V_L = -60$; $V_{Ca} = 120$; $V_K = -80$; $V_1 = -1.2$; $V_2 = 18$; $V_3 = 12$; $V_4 = 17.4$; $\phi = 1/3$; $I = 2$; $a = 1$; $b = 3$; $c = 1$; $d = 5$; $r = 0.001$; $s = 4$; $x_R = -8/5$;

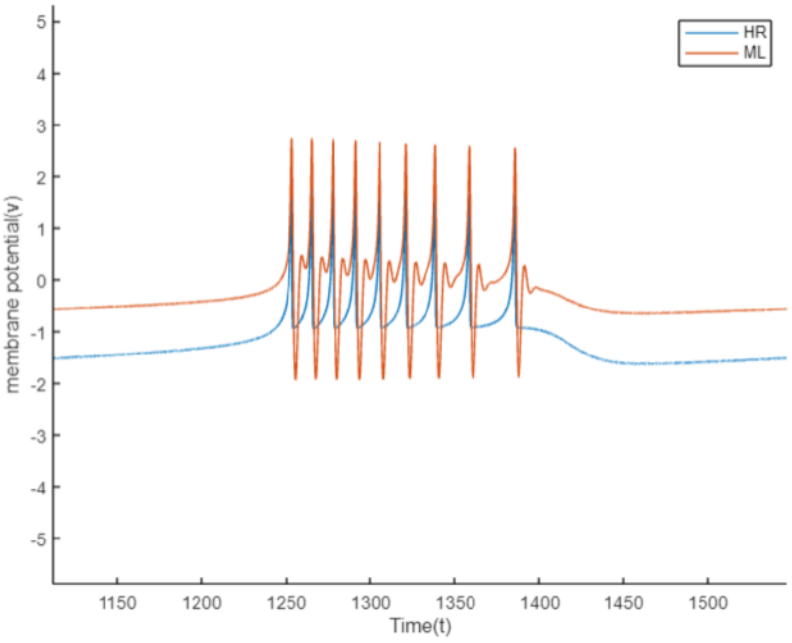

Figure 4.13: Closer look into the $\gamma = 10$ case

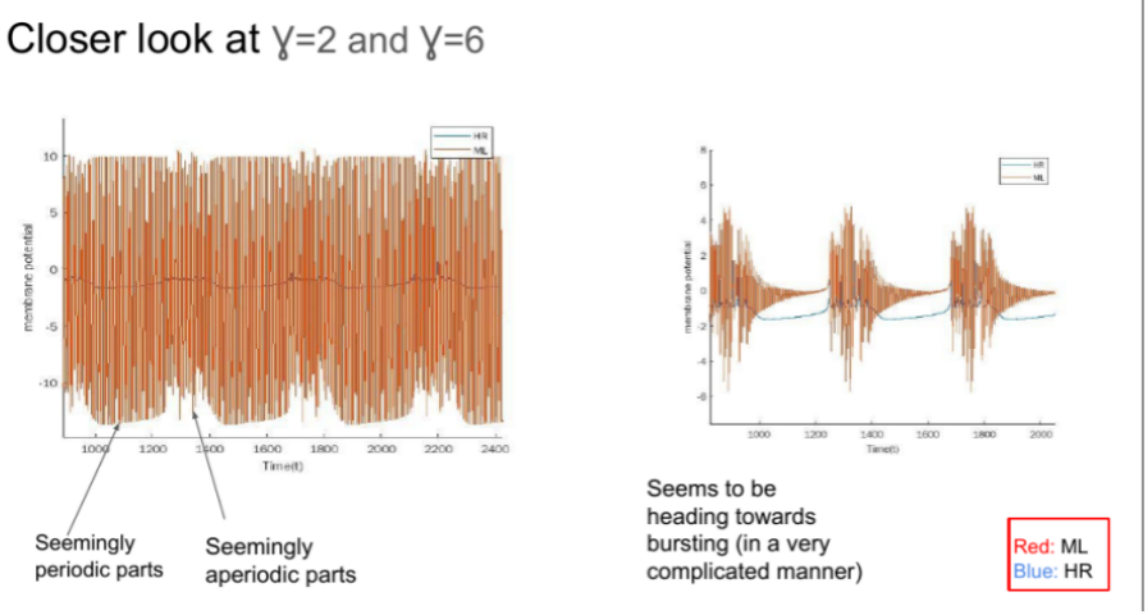

Figure 4.14: Zoomed

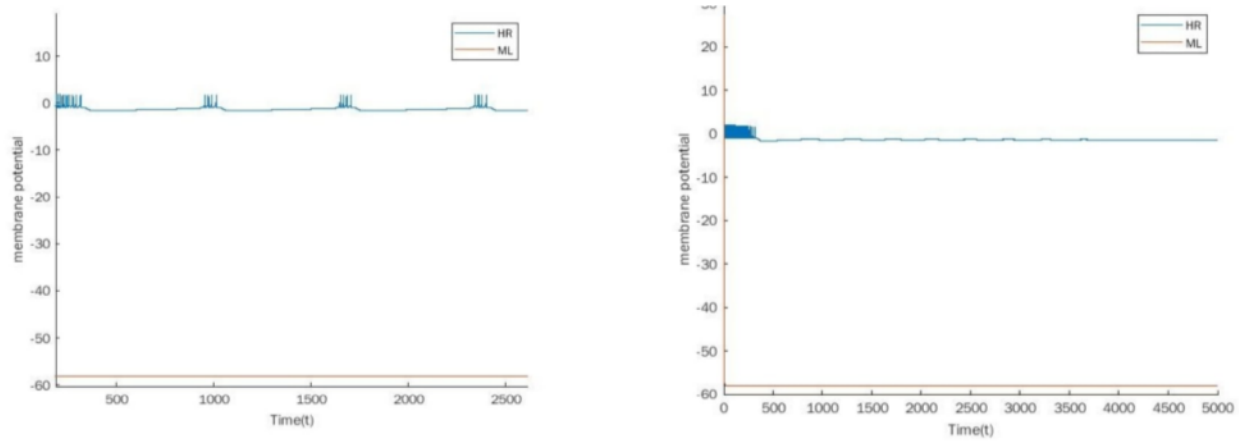

Figure 4.15:
At low gamma, both the neurons burst, but they stop bursting and become quiescent around $\gamma = 0.129$. With parameter values $C = 5$; $g_L = 2$; $g_{Ca} = 4$; $g_K = 8$; $V_L = -60$; $V_{Ca} = 120$; $V_K = -80$; $V_1 = -1.2$; $V_2 = 18$; $V_3 = 12$; $V_4 = 17.4$; $\phi = 1/3$; $I = 2$; $a = 1$; $b = 3$; $c = 1$; $d = 5$; $r = 0.001$; $s = 4$; $x_R = -8/5$;

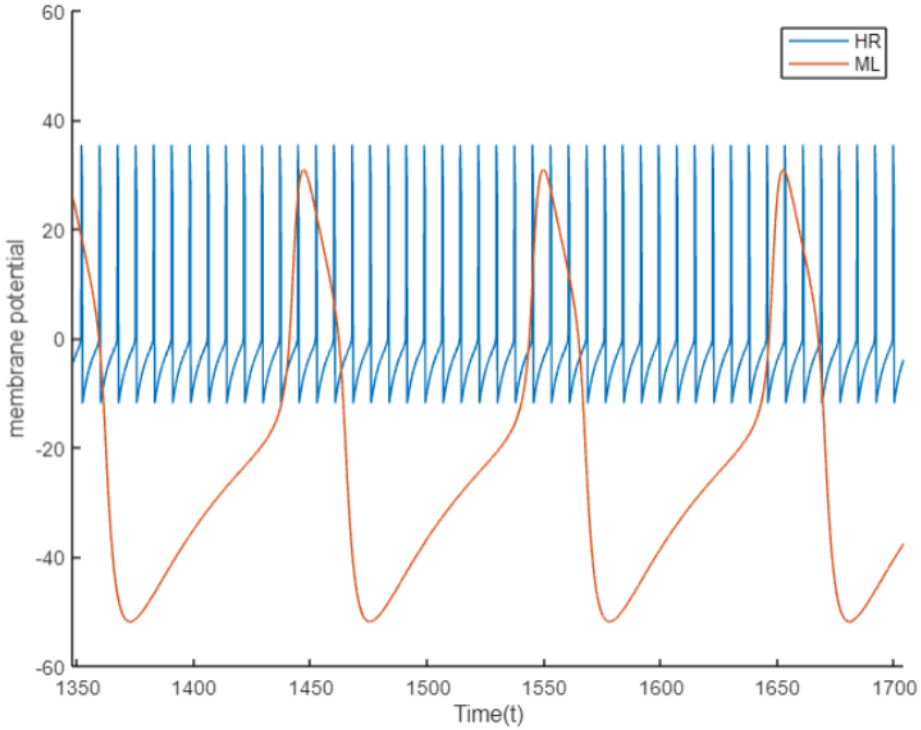

Figure 4.16: Time series plot of the HR and ML neurons (uncoupled) for case 12

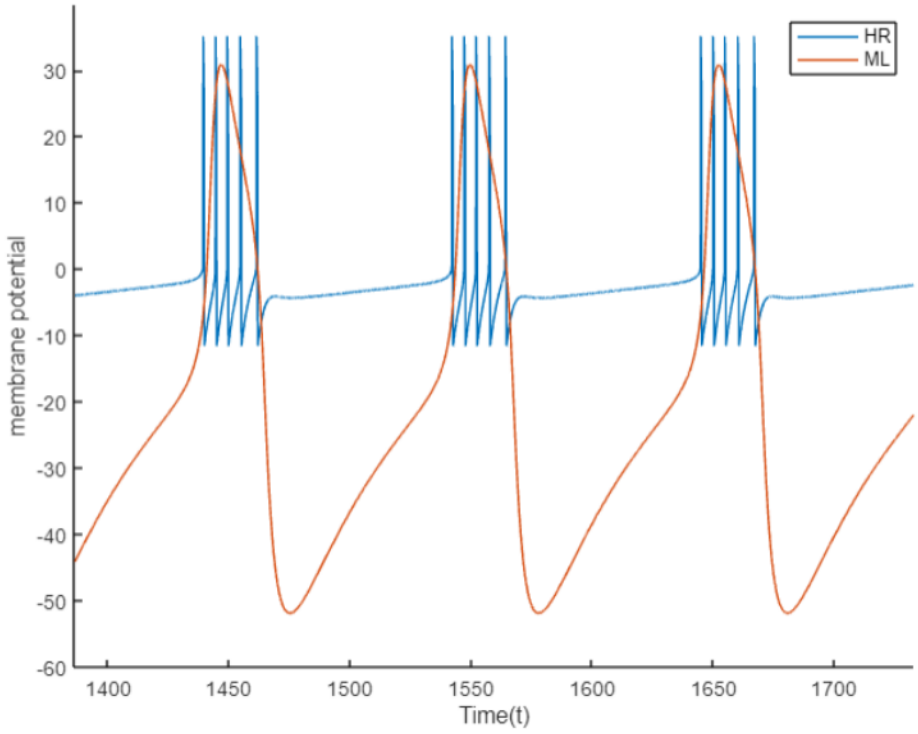

Figure 4.17: Time series plot of the HR and ML neurons (coupled) for case 12

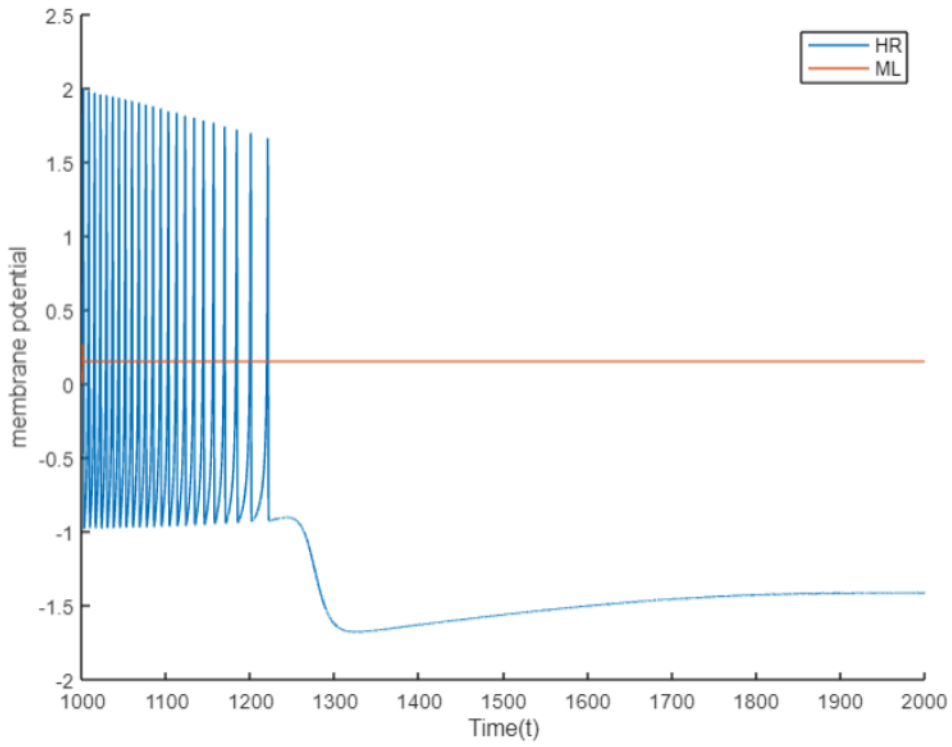

Figure 4.18: Bidirectional case 1, when uncoupled

4.2 Bidirectional Case

4.2.1 Case 1:

This case has the two neurons bidirectionally coupled, with parameters $C = 5$; $g_L = 2$; $g_{Ca} = 4$; $g_K = 8$; $V_L = -60$; $V_{Ca} = 120$; $V_K = -80$; $V_1 = -1.2$; $V_2 = 18$; $V_3 = 12$; $V_4 = 17.4$; $\phi = 1/3$; $I = 2$; $a = 1$; $b = 3$; $c = 1$; $d = 5$; $r = 0.001$; $s = 4$; $x_R = -8/5$.

When uncoupled (Fig 4.18), both the neurons are quiescent. However, on coupling bidirectionally, they both start bursting around $\gamma = 0.818$. Close-up views of the same have been shown in Fig 4.20 and Fig 4.21

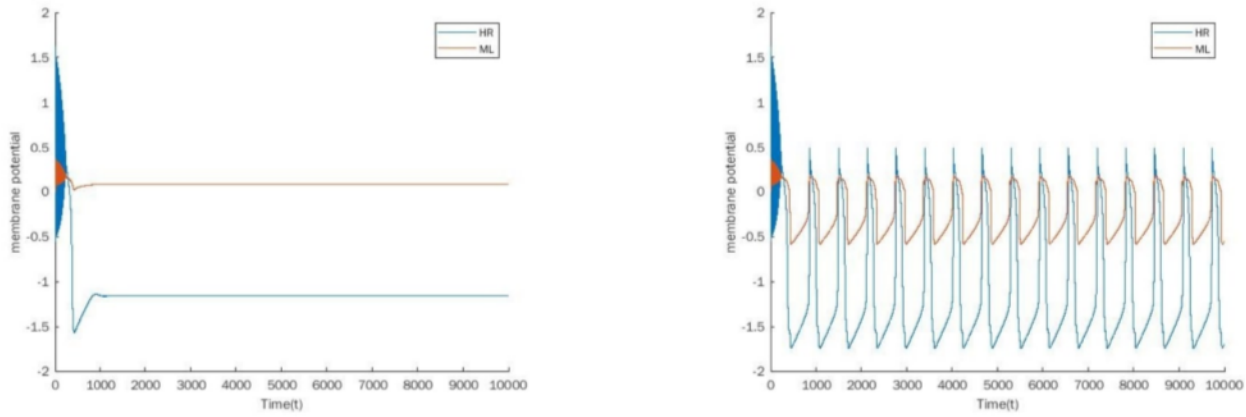

Figure 4.19:
Case 1: Neurons remain quiescent until $\gamma = 0.815$, where it begins periodic spiking abruptly. With parameter values $C = 5$; $g_L = 2$; $g_{Ca} = 4$; $g_K = 8$; $V_L = -60$; $V_{Ca} = 120$; $V_K = -80$; $V_1 = -1.2$; $V_2 = 18$; $V_3 = 12$; $V_4 = 17.4$; $\phi = 1/3$; $I = 2$; $a = 1$; $b = 3$; $c = 1$; $d = 5$; $r = 0.001$; $s = 4$; $x_R = -8/5$;

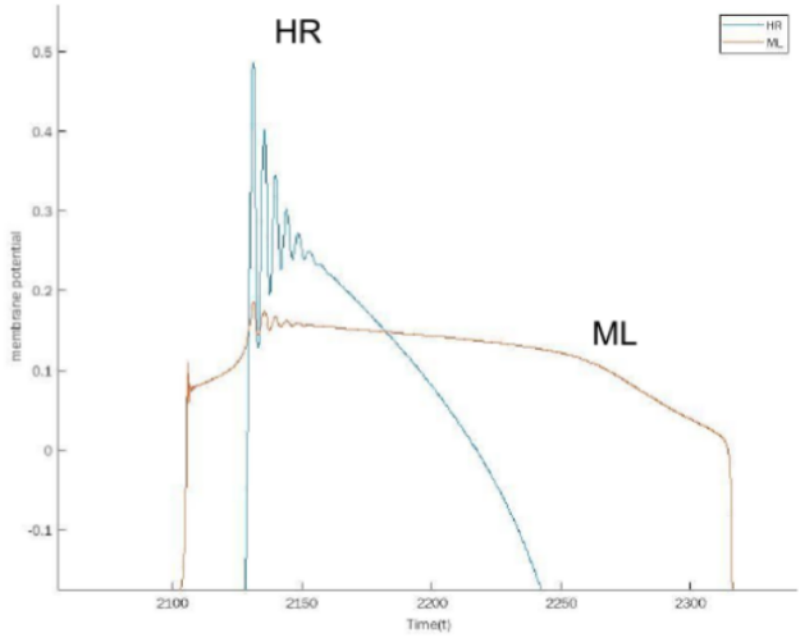

Figure 4.20: Case 1: Zoomed into a single burst

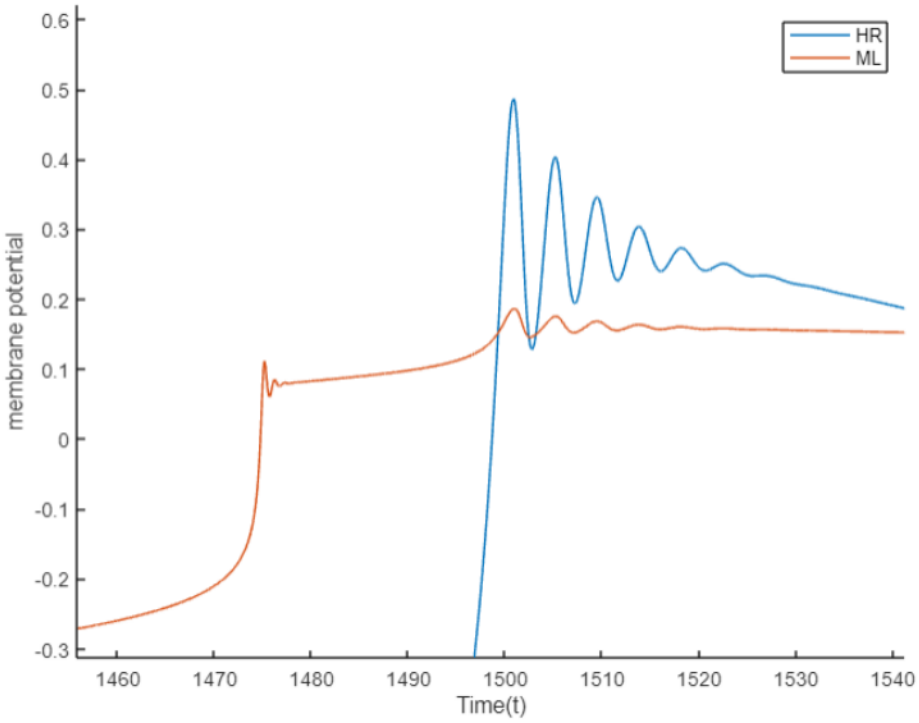

Figure 4.21: Bidirectional Case 1: Even more zoomed

Chapter 5

Conclusion and Further Directions

Firstly, we have covered the basic concepts behind how a neuron is modelled as a dynamical system and how its neurocomputational properties can be derived from the analyses of the dynamical system. We hope this holds some pedagogical value in quickly introducing concepts like bursting, classification of neurons according to excitability, classification of bursting according to the underlying mechanisms etc. We reviewed dynamics of various parameter regimes of the Morris Lecar and the Hindmarsh-Rose neurons extant in literature. we discussed the mechanisms behind various kinds of interesting bursting in the Hindmarsh-Rose neuron. We coupled a neuron capable of both type I and type II activity (ML) to another neuron capable of a large variety of bursting (HR) and examined their dynamics.

We have explored the unidirectional cases in 10 different cases: 5 for type-I ML neuron and 5 for type-II ML neuron. each of those 5 cases correspond to some interesting bursting pattern of the driving HR neuron. We have also explored the underlying bursting mechanism in case 1. In the unidirectional case, we observed bursting in ML neuron in all the cases under the influence of a strong coupling ($\gamma = 10$) and noted that bursting amplitude increases with the strength of coupling. Maybe it's because of the strong coupling that the mechanism deduced in case 1 aligned with that of the driver HR neuron (fold/hom). In the bidirectional case we observed a phenomenon where both neurons stop activity once coupled, though its explanation remains to be explored. In the unidirectional case we observed another case where seemingly aperiodic spiking activity occurs, and its explanation remains to be explored.

Further directions from here may include finding out those explanations, study of synchronisation phenomena in the bidirectionally coupled system, finding out bifurcation mechanisms for the bursts other than case 1, exploring dynamics of the coupled systems in other parameter regimes, and finding out quiescent, spiking and bursting regimes in parameter plots like I vs γ plots in different cases.

Bibliography

[1] Eugene M. Izhikevich 2010, "Dynamical Systems in Neuroscience: The Geometry of Excitability and Bursting", Cambridge, Massachusetts: the MIT Press.

[2] Eugene M. Izhikevich, "Neural Excitability, Spiking and Bursting", Int. J. Bifurcation and Chaos, 10, 1171-1266 (2000).

[3] C. Morris and H. Lecar, quot;Voltage Oscillations in the barnacle giant muscle fiberquot;, Biophys. J. 35, 193-213 (1981).

[4] J. L. Hindmarsh and R. M. Rose,quot;A model of neuronal bursting using three coupled first order differential equationsquot;, Proc. R. Soc. Lond. B 221, 87-102 (1984).

[5] Tsumoto, Kunichika; Kitajimab, Hiroyuki; Yoshinagac, Tetsuya; Aiharad, Kazuyuki; Kawakamif, Hiroshi (January 2006), "Bifurcations in Morris–Lecar neuron model" (PDF), Neurocomputing (in English and Japanese), 69 (4–6): 293–316

[6] Burst mechanisms and burst synchronization in a system of coupled type-I and type-II neurons S De, J Balakrishnan Communications in Nonlinear Science and Numerical Simulation 90, 105391

[7] Lixia Duan, Dehong Zhai, Qishao Lu. Bifurcation and bursting in Morris-Lecar model for class I and class II excitability. Conference Publications, 2011, 2011 (Special) : 391-399. doi: 10.3934/proc.2011.2011.391

[8] Shilnikov, Andrey Kolomiets, Marina. (2008). Methods of the Qualitative Theory for the Hindmarsh-rose Model: a Case Study - a Tutorial.. I. J. Bifurcation and Chaos. 18. 2141-2168. 10.1142/S0218127408021634

[9] Nathalie Corson, Moulay Aziz-Alaoui. Asymptotic dynamics of Hindmarsh-Rose neuronal system. Dynamics of Continuous, Discrete and Impulsive Systemes, Series B: Applications and Algorithms, 2009, p.535. hal-00952598

[10] Roberto Barrio, Santiago Ibáñez, Lucía Pérez, Hindmarsh–Rose model: Close and far to the singular limit, Physics Letters A, Volume 381, Issue 6, 2017, Pages 597-603, ISSN 0375-9601

[11] Innocenti, Giacomo Morelli, Alice Genesio, Roberto Torcini, Alessandro. (2008). Dynamical phases of the Hindmarsh-Rose neuronal model: Studies of the transition from bursting to spiking chaos. Chaos (Woodbury, N.Y.). 17. 043128. 10.1063/1.2818153.

[12] Storace, Marco Linaro, Daniele Lange, Enno. (2008). The Hindmarsh-Rose neuron model: Bifurcation analysis and piecewise-linear approximations. Chaos (Woodbury, N.Y.). 18. 033128. 10.1063/1.2975967.

[13] Hodgkin AL. The local electric changes associated with repetitive action in a non-modulated axon. J Physiol 1948;107:165–81

[14] Hodgkin L, Huxley AF . A quantitative description of membrane current and its application to conduction and excitation in nerve. J Physiol 1952;117:500–44

[15] Izhikevich EM, Hoppensteadt FC. Classification of bursting mappings. Int J Bifurcat Chaos 2004;14(11):3847–54.

[16] Izhikevich EM, Desai NS, Walcott EC, Hoppensteadt FC. Bursts as a unit of neural information: selective communication via resonance. Trends Neurosci 2003;26:161–7.

[17] Cardin JA, Carlen M , Meletis K, Knoblich U, Zhang F, et al. Driving fast-spiking cells induces gamma rhythm and controls sensory responses. Nature 2009;459:663–7.

[18] Bartos M , Vida I, Jonas P. Synaptic mechanisms of synchronized gamma oscillations in inhibitory interneuron networks. Nat Rev Neurosci 2007;8:45–56.